Geothermics 105 (2022) 102537

Contents lists available at ScienceDirect

Geothermics

journal homepage: www.elsevier.com/locate/geothermics

Using multiple partially-penetrating wells (MPPWs) to improve the performance of high-temperature ATES systems: Well operation, storage conditions and aquifer heterogeneity

J.H. van Lopik [a,*], N. Hartog [a,b], R.J. Schotting [b]

[a] KWR Water Research Institute, Groningenhaven 7, 3433 PE Nieuwegein, the Netherlands
[b] Utrecht University, Department of Earth Sciences, Princetonlaan 8, 3584 CB Utrecht, the Netherlands

ARTICLE INFO

Keywords:
Aquifer thermal energy storage (ATES)
Thermal convection
Partially-penetrating wells
Recovery efficiency
Numerical modeling

ABSTRACT

The occurrence of free thermal convection negatively affects thermal recovery efficiencies of High-Temperature Aquifer Thermal Energy Storage (HT-ATES) systems. In this study the potential of applying a Multiple Partially Penetrating Well (MPPW) configuration to counteract the impact for seasonal HT-ATES is tested through numerical modeling with SEAWATv4. For scenarios where the thermal front is close to the HT-ATES well-screen and free thermal convection has considerable effect on the thermal recovery efficiency, the use of a MPPW configuration has great potential. Storage at a moderate temperature contrast ($\Delta T = 40$ °C) between the hot injection volume and cold ambient groundwater in a high-permeability aquifer resulted in significant improvement of the thermal recovery efficiency with a MPPW configuration targeting injection in lower parts of the aquifer and recovery in the upper parts. For conventional, fully screened HT-ATES a thermal recovery efficiency of 0.43 is obtained while this is 0.59 with the MPPW scheme in the first recovery cycle. This recovery efficiency of 0.59 is only 0.11 less than a theoretical case with no buoyancy effects. For seasonal HT-ATES cases that face severe free thermal convection, rapid accumulation of heat in the upper part of the aquifer is observed and the MPPW configuration is less effective due to the long period between injection and recovery. Especially for HT-ATES cases that require a cut-off temperature, thermal recovery can be significantly improved and prolonged. For storage temperatures of 60 and 80 °C in a high-permeability aquifer, approximately 4 times more abstracted usable heat is obtained with the MPPW setup while considering a cut-off temperature of 40 °C. Moreover, the present study shows that the use of MPPW configurations in heterogeneous aquifers should be carefully planned. Improper application of MPPW is particularly vulnerable for simplification of the aquifer characteristics, and therefore proper site heterogeneity investigation and operational monitoring are required to benefit from optimal MPPW operation during HT-ATES.

1. Introduction

In the last decade, the global climate goals (UN, 2015) have accelerated research into the reduction of significant CO_2 emissions by the use of fossil fuels for heating and cooling purposes. For the realization of this ambition, the storage of thermal energy to overcome temporal mismatch between energy demand and supply has shown to be essential (Alva et al., 2018; Dinçer and Rosen, 2021). The use Aquifer Thermal Energy Storage (ATES) has great potential to level these mismatches and is already widely applied (Bloemendal et al., 2015; Fleuchaus et al., 2018). However, to date, most ATES systems operate at relatively low absolute temperatures (LT-ATES, $T<25$ °C), which is too low to allow direct heating of buildings and therefore require additional heating from other sources such as heat pumps. Storage at higher temperatures with HT-ATES (e.g. $T>70$ °C) allows higher energy storage capacities, as well as improvement of the overall energy efficiency of the system. Moreover it allows direct heating without the use of heat pumps and the coupling to a broader range of sustainable heat sources, such as geothermal energy, industrial waste heat, or converted energy from wind turbines and solar panels (Fleuchaus et al., 2020). Although HT-ATES has these benefits, only a limited number of these systems is in operation worldwide (Kabus and Seibt, 2000; Holstenkamp et al., 2017; Fleuchaus et al., 2018, 2020). In the last decade, interest in the suitability and applicability of HT-ATES has grown massively, resulting in many case studies

* **Corresponding author at:** KWR Water Research Institute, KWR Water, Geohydrology, Groningenhaven 7, 3433 PE Nieuwegein, The Netherlands.
E-mail address: jan.van.lopik@kwrwater.nl (J.H. van Lopik).

https://doi.org/10.1016/j.geothermics.2022.102537
Received 6 March 2022; Received in revised form 18 July 2022; Accepted 27 July 2022
Available online 18 August 2022
0375-6505/© 2022 Elsevier Ltd. All rights reserved.

which explore the potential of HT-ATES for site-specific conditions (e.g. Réveillère et al., 2013; Zeghici et al., 2015; Xiao et al., 2016; Opel et al., 2017; Winterleitner et al., 2018; Ueckert and Baumann, 2019; Collignon et al., 2020; Stricker et al., 2020; Van der Roest et al., 2021).

For HT-ATES systems, the occurrence of free thermal convection (buoyancy-driven flow) can be an important intrinsic process negatively affecting thermal recovery efficiencies (Schout et al., 2014; Van Lopik et al., 2016; Sheldon et al., 2021). This is in addition to the heat losses that also occur in LT-ATES systems due to thermal conduction and displacement by ambient groundwater flow (Doughty et al., 1982; Bloemendal and Hartog, 2018). In confined aquifers, these buoyancy-induced heat losses result from the tilting of thermal front due to the density difference between the hot injection water and cooler ambient groundwater (Hellström et al., 1979; Schout et al., 2014). In particular for smaller HT-ATES systems where the thermal front tilting occurs close to the HT-ATES well, as well as for systems where the free thermal convective component will be large, such as in more permeable aquifers and at larger temperature differences, the impact on the thermal recovery efficiency is significant (e.g., Molz et al., 1983a, b; Buscheck et al., 1983; Schout et al., 2014; Van Lopik et al., 2016, Sheldon et al., 2021).

Depending on the system requirements and the hydrogeological characteristics of the subsurface, shortening of the storage time, a storage volume increase or an available, thinner storage aquifer might be considered for some cases to reduce the impact of thermal front tilting on the thermal recovery efficiency (Schout et al., 2014; Sheldon et al., 2021). Also the selection of a less (vertically) permeable storage aquifer or a smaller difference between storage and ambient groundwater temperatures might be considered, (e.g. Doughty et al., 1982; Schout et al., 2014), but this comes with trade-offs such as reduced well capacities and lower energetic performance. A numerical study by Van Lopik et al. (2016) showed that the recovery efficiency of HT-ATES systems affected by free thermal convection can be improved significantly by storing the hot water at a higher salinity to compensate the density difference with the cooler ambient groundwater. However, regulatory permission may be difficult to obtain, particularly for storage in aquifers with fresh groundwater resources. Instead of using the density difference compensation method to minimize the effects of buoyancy-driven flow, it can be counteracted hydraulically using Multiple Partially Penetrating Wells (MPPWs) in HT-ATES systems. Implementation of PPWs has already shown to be beneficial for aquifer storage and recovery of fresh water in brackish aquifers (Maliva and Missimer, 2010; Zuurbier et al., 2014; Witt et al., 2021).

The experimental HT-ATES field study of Molz et al. (1983a) and the numerical study of Buscheck et al. (1983) already showed that using a partially-penetrating well (PPW) targeting thermal recovery in the upper part of the highly permeable aquifer in their pilot study can improve the thermal recovery efficiency. In this field pilot a recovery cycle of 140 days of injection, 30 days of storage and 55 days abstraction was applied and significant free thermal convection occurred at injection temperatures of 80 °C. Buscheck et al. (1983) showed numerically that a thermal recovery efficiency of only 0.40 is obtained, while recovery with a PPW in the upper part of the aquifer resulted in thermal recovery efficiencies up to 0.50. However, so far, studies have not considered how the use of MPPWs can further improve recovery efficiencies for fully operational seasonal HT-ATES systems. Different MPPW well operation schemes likely have different impacts on HT-ATES performance, since heat transport by free and forced convection is affected by storage conditions and aquifer characteristics (Schout et al., 2014; Van Lopik et al., 2016). Moreover, HT-ATES systems might require a cut-off temperature for the supplied heat to district heating networks or industries and in such case the quality of the heat becomes an important factor. Hence, besides the potential overall improvement of the thermal recovery efficiency, targeted recovery with MPPWs instead of using a conventional, fully screened well might potentially also prolong the recovery of heat above a given cut-off temperature.

Therefore, in this study, the potential of applying MPPWs for seasonal HT-ATES systems to improve thermal recovery efficiency is investigated numerically for a range of aquifer and storage characteristics, as well as various types of well operation schemes during injection and recovery. Specifically, this study explores the potential of MPPWs designs by numerical density-driven flow simulations of: *(a)* conventional, fully screened HT-ATES systems (Fig. 1a-c), *(b)* HT-ATES systems with various types of MPPW designs enabling injection and/or abstraction in the upper, middle and/or lower part of the aquifer (e.g. Fig. 1d) and *(c)* theoretical HT-ATES cases assuming no density differences between hot injection water and cold ambient groundwater (no free convection) under conventional, fully screened HT-ATES conditions. The latter scenario provides the theoretic achievable thermal recovery efficiency as an upper bound for seasonal HT-ATES systems where buoyancy impact is fully overcome. Firstly, different operational MPPW schemes are numerically tested for homogeneous anisotropic aquifer conditions by simulating multiple seasonal recovery cycles. Secondly, the performance of different MPPW operational schemes is tested in scenarios that consider vertical variability in hydraulic conductivity.

2. Material and methods

2.1. SEAWAT: buoyancy-driven flow and heat transport model

The SEAWATv4 code is used to simulate heat transport and buoyancy-driven and viscosity-dependent groundwater flow during the seasonal HT-ATES recovery cycles (Guo and Langevin, 2002; Langevin et al., 2008). SEAWATv4 is a combined simulation code of MODFLOW (Harbaugh et al., 2000) and MT3DMS (Zheng and Wang, 1999) that solves the coupled groundwater flow and solute transport equations. The differential equations for solute transport can be easily translated into terms of heat transport, following the approach of Langevin et al. (2008).

A non-linear density equation of state is used to describe the fluid density as a function of the groundwater temperature properly. This is done by using the adjusted SEAWATv4 code of Van Lopik et al. (2015) with the empirical non-linear temperature-density relationship of Sharqawy et al. (2010):

$$\rho(T) = \left(999.9 + 2.034{\cdot}10^{-2}T - 6.162{\cdot}10^{-3}T^2 + 2.261{\cdot}10^{-5}T^3 - 4.657{\cdot}10^{-8}T^4\right) \quad (1)$$

where ρ [kg/m^3] is the fluid density and T [°C] is the temperature of the water.

The fluid viscosity as a function of temperature is described by Voss (1984):

$$\mu(T) = 2.394{\cdot}10^{-5}{\cdot}\left(10^{\frac{248.37}{T+133.15}}\right) \quad (2)$$

where μ [kg/(m s)] is the dynamic fluid viscosity.

2.2. Numerical modeling of HT-ATES

2.2.1. General model description: discretization and boundary conditions

An axi-symmetric model domain with a radial extent of 500 m and a thickness of 40 m is constructed following the approach of Langevin (2008). The aquifer thickness is 21 meter, and the over- and underlying aquitards are respectively 10 and 9 meter thick. The grid resolution is Δr=0.5 and Δz=0.5 m. Several numerical tests at different grid resolutions were run, which showed that this resolution was sufficient. Constant head and temperature are used for the outer, upper and lower boundaries of the model domain.

The MPPW is located in the center of the axisymmetric model domain, with impermeable cells at aquitard depths and at the non-screened parts between the PPWs. The PPWs with a screen length of

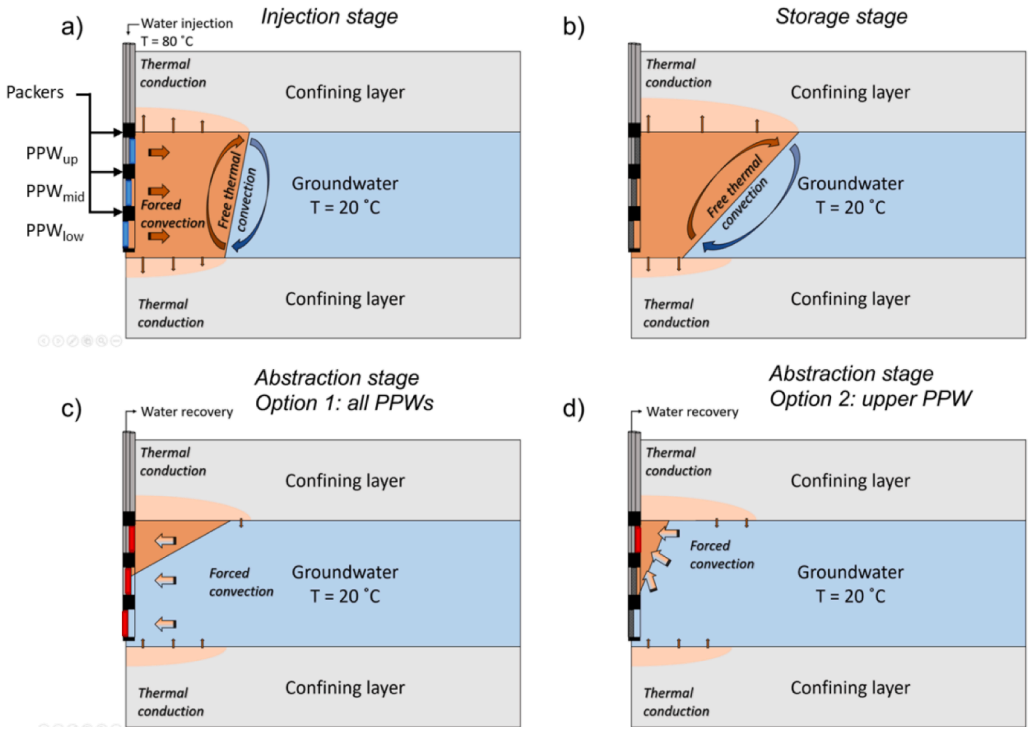

Fig. 1. Schematic overview of a full HT-ATES recovery cycle in a confined aquifer with a MPPW configuration for **a)** injection (operative injection PPW screens are blue), **b)** storage. For abstraction stage, two different options for well operation are shown, with **c)** conventional, abstraction over the entire thickness of the aquifer by the upper, middle and lower PPWs, **d)** and a well operation example with abstraction in only the upper PPW. The operative injection PPW screens are red.

5 meter and a radius of 0.1 m are screened at different aquifer depths: (a) the *upper* PPW at 11<z<16 m, (b) the *middle* PPW at 18<z<23 m and (c) the *lower* PPW at 25<z<30 m). This MPPW configuration is used for all simulated well operation scheme scenarios.

The Preconditioned Conjugate Gradient 2 (PCG2) package is used for simulating groundwater flow, and the modified method of characteristics (MMOC) with a Courant number of 0.2 is used as advection package for heat transport. The convergence criterion of relative temperature was set to 10^{-10} to solve heat transport by conduction accurately (Vandenbohede et al., 2014).

2.2.2. Characteristics and conditions of the generalized HT-ATES cases

The present study numerically investigates the potential of improving the thermal recovery efficiency during seasonal HT-ATES by using the described MPPW configuration. The characteristics of the homogeneous anisotropic aquifer listed in Table 1 are used to model the *base case* (Case 1) of the sensitivity analysis. These characteristics are based on the aquifer of the Auburn University (USA) field experiment (Molz et al., 1983a; Buscheck et al., 1983). A seasonal HT-ATES system is assumed, with equal injection, storage, abstraction and rest periods of 90 days. Four consecutive recovery cycles are assumed for all simulated scenarios with equal injection and abstraction volumes for each cycle.

A sensitivity analysis is conducted to explore the performance of various aquifer and storage characteristics (Table 2). For each case in the sensitivity analysis eight different HT-ATES well scheme scenarios are simulated with *(a)* a reference well operation setup with conventional, fully screened HT-ATES considering equal injection and abstraction rates in all three PPWs, *(b)* six different setups to test various injection and abstraction well operation schemes with the MPPW configuration as shown in Table 3, and *(c)* a setup under theoretical condition of no free convection (*nfc*).

The six setups with different injection and abstraction schemes investigate the differences in HT-ATES performance when infiltrating only in the lower parts of the aquifer, as well as abstracting only in the upper parts of the aquifer with the proposed MPPW configuration.

Table 1
Aquifer and aquitard properties of the Auburn University field experiment (Molz et al., 1983a). *The thermal distribution coefficient (K_{dT}), thermal retardation factor (R_T), bulk thermal diffusivity (D_T) are calculated for SEAWATv4 heat transport simulation (see Langevin et al., 2008).

Aquifer properties	Parameter values
Specific storage	$S_s = 6{\cdot}10^{-4}$ m^{-1}
Porosity	$\theta = 0.25$
Bulk density	$\rho_b = 1950$ kg/m^3
Heat capacity	$c_{ps} = 696.15$ J/kg °C
Thermal conductivity	$\lambda_s = 2.29$ W/m °C
Thermal distribution coefficient*	$K_{dT} = 1.66{\cdot}10^{-4}$ m^3/kg
Thermal retardation factor*	$R_T = 2.29$
Bulk thermal diffusivity*	$D_T = 0.189$ m^2/day
Overall horizontal hydraulic conductivity	$k_h = 53.4$ m/day
Overall vertical hydraulic conductivity	$k_v = 7.7$ m/day
Aquifer thickness	$H_a = 21$ m
Longitudinal dispersion	$\alpha_l = 0.5$ m
Transversal dispersion	$\alpha_t = 0.05$ m
Aquitard properties	
Specific storage	$S_s = 9{\cdot}10^{-2}$ m^{-1}
Porosity	$\theta = 0.35$
Bulk density	$\rho_b = 1690$ kg/m^3
Heat capacity	$c_{ps} = 696.15$ J/kg °C
Thermal conductivity	$\lambda_s = 2.56$ W/m °C
Thermal distribution coefficient*	$K_{dT} = 1.66{\cdot}10^{-4}$ m^3/kg
Bulk thermal diffusivity*	$D_T = 0.151$ m^2/day
Horizontal hydraulic conductivity	$k_h = 53.4{\cdot}10^{-5}$ m/day
Vertical hydraulic conductivity	$k_v = 7.7{\cdot}10^{-5}$ m/day
Upper aquitard thickness	$H_{up} = 10$ m
Lower aquitard thickness	$H_{low} = 9$ m
Groundwater properties	
Heat capacity of the fluid	$c_{pf} = 4186$ J/kg °C
Thermal conductivity of the fluid	$\lambda_l = 0.58$ W/m °C

Table 2
Summary of the input parameters used for the sensitivity analysis. Bold values with an asterisk (*) indicate a variation on the *base case* (Case 1).

	K_h [m/day]	K_v [m/day]	a=K_h/k_v	T_{in} [°C]	V_{in} [m^3]	r_{th} [m]
Case 1	53.4	7.7	6.9	80	56,700	38.8
Case 2	53.4	7.7	6.9	***60****	56,700	38.8
Case 3	***15****	***1.5****	***10****	80	56,700	38.8
Case 4	53.4	7.7	6.9	80	***28,350****	27.4
Case 5	53.4	7.7	6.9	80	***113,400****	54.8

Table 3
Summary of the simulated well operation schemes with the MPPW configuration for Cases 1–3. Note that for Case 4 and 5, the volumetric flow rates per PPW are respectively a factor 2 lower and higher.

Well operation scheme	Volumetric flow rate per PPW during injection [m^3/h]			Volumetric flow rate per PPW during recovery [m^3/h]		
	Upper	*Middle*	*Lower*	*Upper*	*Middle*	*Lower*
Fully screened (Ref.)	8.75	8.75	8.75	−8.75	−8.75	−8.75
Scheme a	8.75	8.75	8.75	−26.3	0	0
Scheme b	8.75	8.75	8.75	−13.1	−13.1	0
Scheme c	0	13.1	13.1	−26.3	0	0
Scheme d	0	13.1	13.1	−13.1	−13.1	0
Scheme e	0	0	26.3	−26.3	0	0
Scheme f	0	0	26.3	−13.1	−13.1	0

2.2.3. Characteristics and conditions of HT-ATES cases in stratified heterogeneous aquifers

For the simulated heterogeneous cases, the average horizontal and vertical hydraulic conductivities are equal to the equivalent homogeneous anisotropic aquifer conditions of the *base case* (Case 1, see Table 4). The heterogeneous aquifers consist of three layers of 7 m thickness with each its specific hydraulic characteristics. The average horizontal hydraulic conductivity $K_{h,av}$ of a heterogeneously layered aquifer is calculated by (Kasenow, 2010):

$$K_{h,av} = \frac{\sum K_{h,i} H_i}{H_{tot}} \tag{3}$$

where H_{tot} [m] is the aquifer thickness, H_i [m] the thickness of layer *i*, $K_{h,i}$ [m/day] the horizontal hydraulic conductivity of layer *i*.

The average vertical hydraulic conductivity $K_{z,av}$ is calculated by:

$$K_{z,av} = \frac{H_{tot}}{\sum \frac{H_i}{K_{z,i}}} \tag{4}$$

where $K_{v,i}$ [m/day] is the vertical hydraulic conductivity of layer *i*.

Equal well heads for the active PPWs are assumed during injection and abstraction to obtain the required volumetric flow rate of 26.3 m^3/h. Therefore, injection and abstraction rates of the individual PPWs in different aquifer layers are set proportional to the hydraulic conductivities of the screened aquifer layers.

Table 4
The horizontal and vertical hydraulic conductivities of the simulated heterogeneous aquifers.

	Heterogeneous aquifer conditions			
	Layer	H_a [m]	K_h [m/day]	K_v [m/day]
Case H.1	L1	7	75	25
	L2	7	10	3.25
	L3	7	75	25
Case H.2	L1	7	75	25
	L2	7	75	25
	L3	7	10	3.25
Case H.3	L1	7	10	3.25
	L2	7	75	25
	L3	7	75	25
Case H.4	L1	7	10	5.3
	L2	7	140	72
	L3	7	10	5.3
Case H.5	L1	7	10	5.3
	L2	7	10	5.3
	L3	7	140	72
Case H.6	L1	7	140	72
	L2	7	10	5.3
	L3	7	10	5.3

2.3. Quantification of thermal energy recovery and thermal front tilting

The thermal recovery efficiency (ε_H) is defined as the ratio between the total injected heat (Q_{in}) in the PPWs and the total recovered heat (Q_{abs}) from the PPWs:

$$\varepsilon_H = \frac{Q_{abs}}{Q_{in}} = \frac{\sum\left(V_{abs}\ \rho_{abs}(T,S)\ c_{pf}\ (T_{abs} - T_a)\right)}{\sum\left(V_{in}\ \rho_{in}(T,S) c_{pf}\ (T_{in} - T_a)\right)} \tag{5}$$

where $V_{abs/in}$ [m^3] are the volumes per time step of the abstracted water and the injected water, $T_{abs/in}$ [°C] the temperatures of the abstracted water and the injected water, T_a [°C] the ambient groundwater temperature, c_{pf} [J/(kg °C)] the specific heat of water and $\rho_{abs/in}$ (T) [kg/m^3] the densities of the abstracted water and the injected water as a function of temperature (Eq. (1)). The average temperature over time of the recovered hot water in the PPWs is calculated and used to obtain the total recovered heat.

Considering the stored hot water volume for a fully screened HT-ATES system in a confined aquifer while ignoring heat loss by free convection, cylindrical dimensions can be assumed for the stored hot water volume with a maximum radial extent of the hot water (r_{th}) for a given aquifer thickness (H_a). These dimensions are listed in Table 2 for the simulated cases in the sensitivity analysis. The maximum radial extent of the hot injection water (r_{th}) is defined as:

$$r_{th} = \sqrt{\frac{V_{in}}{\pi\ H_a\ \theta\ R_T}} \tag{6}$$

where θ [-] is the porosity, H_a [m] is confined aquifer thickness and R_T [-] is the thermal retardation factor:

$$R_T = 1 + \frac{\rho_b}{\theta}\frac{c_{ps}}{\rho_f c_{pf}} \tag{7}$$

where ρ_b [kg/m^3] is the dry bulk density and c_{ps} [J/(kg °C)] is the specific heat of the solid.

3. Results

The results in this study are presented in three parts. Firstly, the performances of HT-ATES with the different well operation schemes for the *base case* (Case 1) are presented. Secondly, the sensitivity analysis for different storage and aquifer conditions (Cases 2–5) are presented. Finally, HT-ATES performance in six different heterogeneous-layered aquifers (Cases H.1–6) is evaluated.

3.1. Base case: Auburn university aquifer with homogeneous anisotropic conditions (Case 1)

Under conventional, fully screened well operation (Case 1.*ref*) in the high-permeability aquifer of the *base case* the lowest recovery efficiency is obtained (Fig. 2). The simulated recovery efficiency is only 0.30 after cycle-1 and 0.39 after cycle-4, which is identical to the simulation results of Van Lopik et al. (2016) with a fully-penetrating HT-ATES well. The results of the different well operation schemes (Cases 1.*a-f*, see Table 3) show that the thermal recovery efficiencies are improved, compared to fully screened well operation. Overall, the scenarios with abstraction in

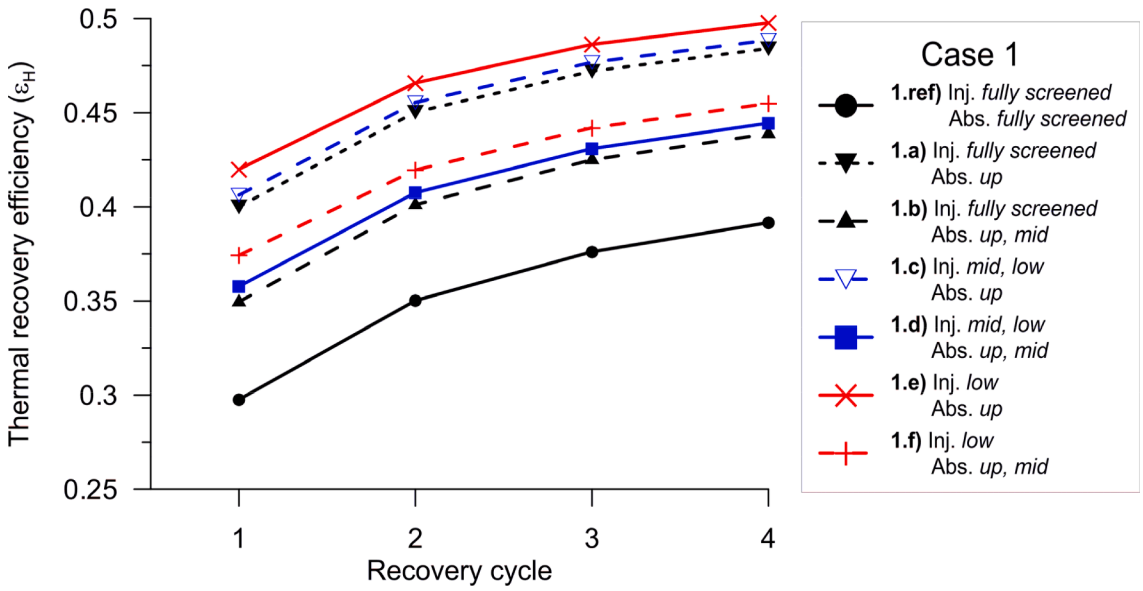

Fig. 2. Calculated thermal recovery efficiency per cycle for the *base case* (Case 1).

only the upper PPW during recovery (Cases 1.*a*, 1.*c* and 1.*e*) resulted in the highest recovery efficiencies. Of the different MPPW schemes tested, Case 1.*e*, where injection occurs in the lower PPW and abstraction in the upper PPW, performed best with a recovery efficiency of 0.42 after cycle-1. Hence, the improvement in thermal recovery efficiency ($\Delta\varepsilon_H$) for Case 1.*e* compared to fully screened well operation (Case 1.*ref*) is +0.12. The improvement in thermal recovery efficiency for Case 1.*b*, where injection occurs in all PPWs and abstraction in the upper two PPWs, is relatively small with a thermal recovery efficiency of only 0.34 for cycle-1. Fig. 2 shows that the selection of the different well operation schemes instead of fully screened HT-ATES is also beneficial after four consecutive years. For Case 1.*e*, a thermal recovery efficiency of 0.50 and an improvement ($\Delta\varepsilon_H$) of +0.11 is obtained compared to fully screened well operation (Case 1.*ref*) after cycle-4.

Due to the high vertical hydraulic conductivity of the aquifer (K_v = 7.7 m/d), and the relatively large temperature contrast (ΔT = 60 °C) in this *base case*, strong free thermal convection is observed during infiltration and storage under fully-screened conditions as shown in Fig. 3a-c and 4a-c. Logically, this also occurs while infiltrating in only the lower part of the aquifer (Case 1.*e*), as shown in Fig. 3d-f and 4d-f. During injection of hot water in only the *lower* PPW, immediate upward heat transport from the lower part of the aquifer towards the non-screened, overlying parts of the aquifer by both free and forced (mixed) thermal convection occurs (Fig. 3d). It takes approximately 45 days to transport the hot water volume over the entire thickness of the aquifer. As a consequence, tilting by lateral heat transport below the upper confining layer does not occur immediately in the injection stage (Fig. 3e), but starts halfway the injection stage when the hot water volume reaches the top of the aquifer (Fig. 3f). This still results in significant residual of accumulated heat in the upper part of the aquifer and in the overlying confining layer after recovery with the upper PPW in Case 1.*e* (Fig. 4f). Hence, the difference in thermal recovery efficiency between HT-ATES with the best performing MPPW scheme (Case 1.*e*) at 0.42 and the theoretical case with no free thermal convection (Case 1.*nfc*) at 0.71 remains large for seasonal HT-ATES in this high-permeability aquifer at a storage temperature of 80 °C.

3.2. Sensitivity analysis

3.2.1. Impact of the MPPW schemes on the thermal recovery efficiency

Fig. 5 shows the thermal recovery efficiencies for all simulated cases in the sensitivity analysis. For HT-ATES at a smaller temperature contrast, the improvement in thermal recovery efficiency with the best performing MPPW scheme (Case 2.*c* with ε_H of 0.59) compared to fully screened HT-ATES (Case 2.*ref* with ε_H of 0.43) is significantly higher than is observed in the *base case* for cycle-1. In this case the improvement ($\Delta\varepsilon_H$) is +0.16, while this is only +0.12 for Case 1 (Table 5). This thermal recovery efficiency is also much closer to the theoretical case with no free thermal convection, resulting in a difference ($\Delta\varepsilon_H$) of only −0.11 while this difference is −0.29 for the *base case* (Table 5). At a lower temperature contrast, the buoyancy component is significantly lower than in the *base case*, which logically results in much higher calculated thermal recovery efficiency for all tested well operation schemes ($0.43 < \varepsilon_H < 0.59$ in cycle-1). For example, during injection in only the lower PPW in Case 1.*e*, the hot water is vertically transported by free thermal convection up to the top of the aquifer within 45 days, while for Case 2.*e* the vertical transport lasts 100 days. Therefore, accumulation of heat in the upper part of the aquifer starts much later.

These effects are even more pronounced in Case 3, where vertical heat transport by free thermal convection is even more restricted due to the low vertical hydraulic conductivity of 1.5 m/d of the aquifer. For example, injection in only the lower PPW (Case 3.*e*) results in no thermal front tilting by lateral heat transport below the upper confining layer in the storage stage, since the hot water volume is not transported into the upper part of the aquifer after 180 days. Due to the low impact of free thermal convection on thermal recovery efficiency in the low-permeability aquifer, the best performing MPPW scheme in the low permeability aquifer (Case 3.*f*), which includes injection in the lower PPW and abstraction in the upper two PPWs, results in only a relative small thermal recovery efficiency improvement ($\Delta\varepsilon_H$) of +0.07 (Table 5).

For the scenarios with a smaller storage volume compared to Case 1, the lowest recovery efficiencies ($0.23 < \varepsilon_H < 0.31$ for Case 4) for conventional HT-ATES are obtained for all recovery cycles. The improvement in thermal recovery efficiency with infiltration in the lower PPW and abstraction in the upper PPW (Case 4.*e*) is slightly higher than in the *base case* (Case 1.e) with a $\Delta\varepsilon_H$ of +0.13 (Table 5). The difference in thermal recovery efficiency between the best performing scenario (Case 4.*e*) and the theoretical case with no free thermal convection ($\Delta\varepsilon_H$ = −0.31) remains huge and is almost similar to the *base case*. For a larger injection volume (Case 5), the improvement of the thermal recovery efficiency with infiltration in the lower PPW and abstraction in the upper PPW is small (Case 5.*e* with $\Delta\varepsilon_H$ of only +0.09). In this scenario, the thermal radius of influence of 54.8 m is higher than in the *base case*

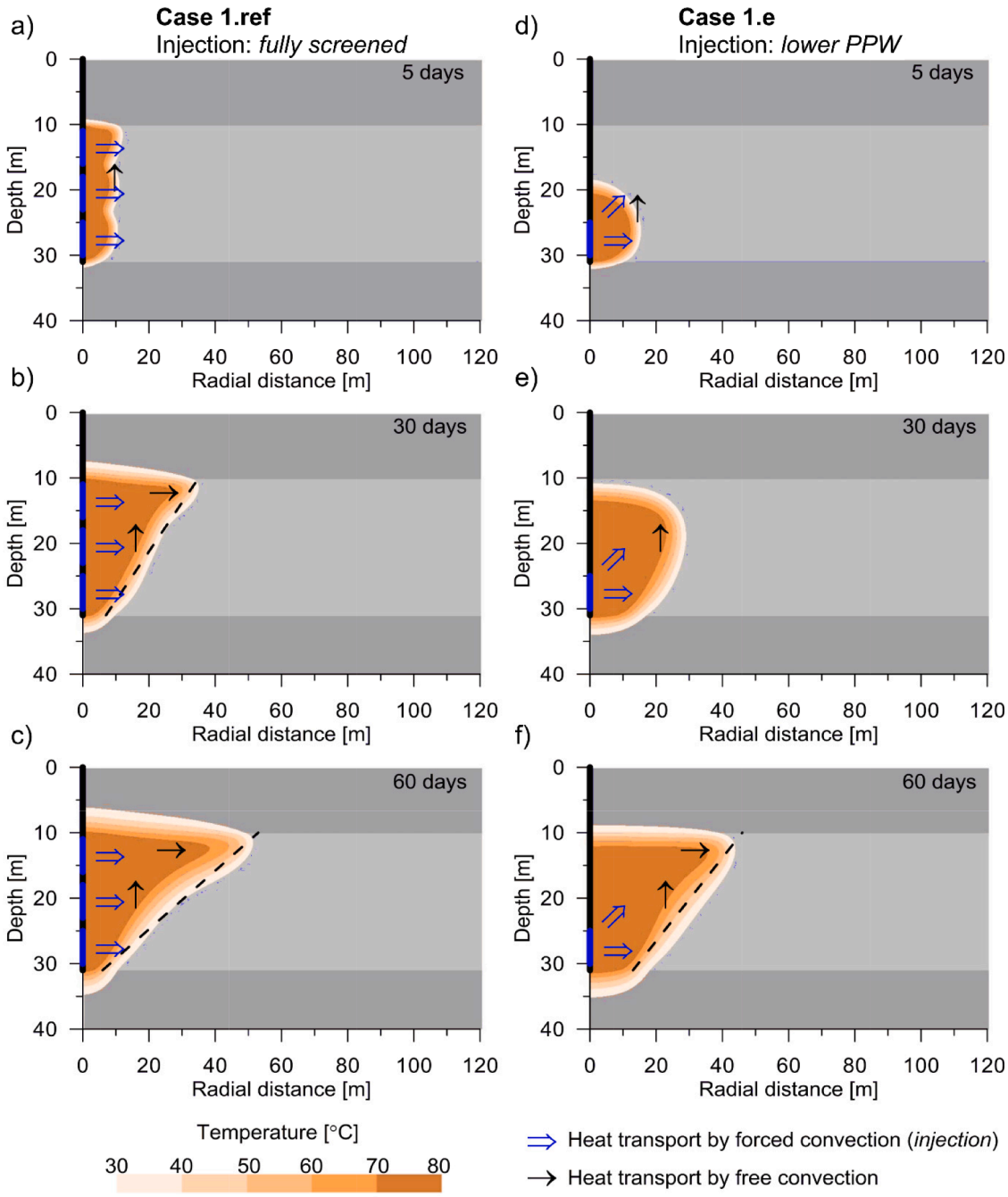

Fig. 3. The temperature distribution contour lines in the aquifer for conventional HT-ATES (Case 1.*ref*) during injection are shown after **a)** 5 days, **b)** 30 days and **c)** 60 days. Similarly, the temperature distribution contour lines in the aquifer are shown for a scenario with injection in only the lower PPW (Cases 1.*e*) after **d)** 5 days, **e)** 30 days and **f)** 60 days. Thermal front tilting is indicated by the dashed line.

(38.8 m for Case 1, see Table 2). As a consequence, the effect of free thermal convection occurs at a large radial distance from the PPW screens and heat loss by free convection has a lower impact on the recovery efficiency. Larger storage volumes in a given target aquifer, but also smaller aquifer thicknesses for a given storage volume, will result in a smaller impact on heat loss by free thermal convection, and therefore reduces the potential benefit of using MPPW configurations.

3.2.2. *Usable heat and cut-off temperature*

Fig. 6 shows that the production temperature and recovered heat over time is significantly lower for fully screened HT-ATES, compared to their best performing MPPW scheme for all simulated cases. However, for the scenarios where water is stored at a temperature of 80 °C (Cases 1 and 4–5), the production temperatures over time for the scenarios with the best performing MPPW scheme are still significantly lower than that of the theoretical scenarios with no free thermal convection (Fig. 6a,d, e). The production temperatures over time can be significantly improved with a MPPW configuration. In cycle-1 of the *base case,* the production temperatures range between 64 and 36 °C during the well operation scheme of injection in the lower PPW and abstraction in the upper PPW (Case 1.*e*), while the production temperatures range only between 48 and 33 °C for fully screened HT-ATES (Case 1.*ref*).

This means that the potential of MPPWs can be much higher if HT-ATES is not only restricted by the overall thermal recovery efficiency as calculated by Eq. (5), but also by the usable heat that is defined by a given cut-off temperature of the system. For example, if a system

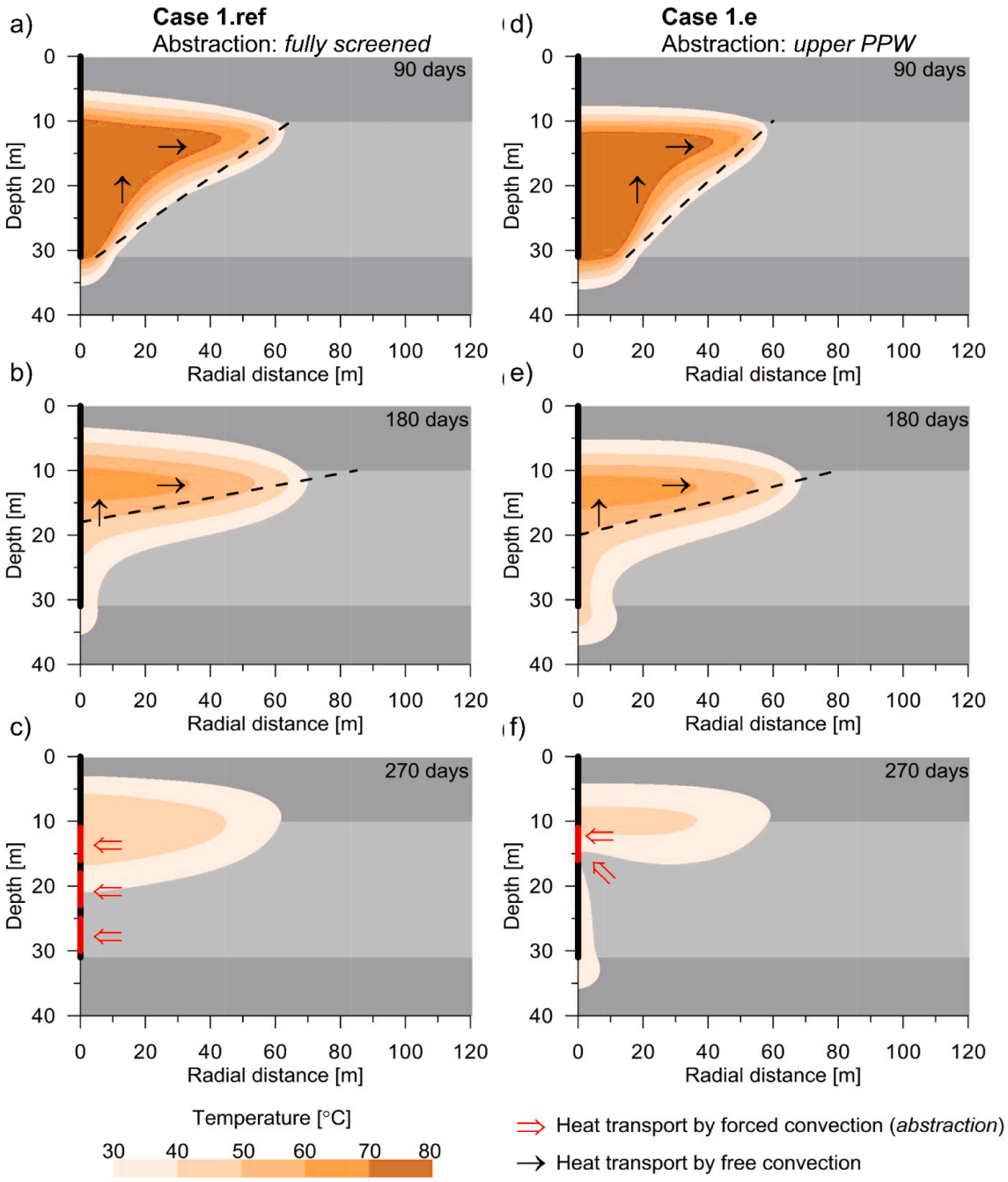

Fig. 4. The temperature distribution contour lines in the aquifer for conventional HT-ATES (Case 1.*ref*) during storage and abstraction are shown after **a)** 90 days (end of injection stage), **b)** 180 days (end of storage stage) and **c)** 270 days (end of recovery stage). Similarly, the temperature distribution contour lines in the aquifer are shown for Case 1.*e* (with injection in the upper, and abstraction in the lower PPW) during storage and abstraction stage after **d)** 90 days (end of injection stage), **e)** 180 days (end of storage stage) and **f)** 270 days (end of recovery stage). Thermal front tilting is indicated by the dashed line.

requires a cut-off temperature of 40 °C, usable heat can only be abstracted for 20 days with the simulated fully screened HT-ATES configuration. After 20 days the production temperatures fall below the cut-off temperature (Fig. 6a). This results in a small amount of recovered usable heat of 1171 GJ. Fig. 6a shows that thermal recovery can be extended up to 60 days with the best performing MPPW scheme (Case 1.*e*), resulting in 3.8 times larger amount of usable heat (4461 GJ, Table 6).

A similar improvement is found for the injection temperature of 60 °C (Case 2), where the recovered usable heat obtained is increased by a factor 3.5 with the best performing MPPW scheme (Case 2.*c*). In fact, the production temperatures over time in this case are close to the theoretical scenario with no free thermal convection (Fig. 6b).

3.2.3. *Decoupled heat recovery over aquifer depth with MPPWs*

In this section the efficiency of decoupled heat recovery with the MPPW configuration is evaluated for the *base case,* while considering fully screened injection and abstraction (Case 1.*ref*). The advantage of a MPPW configuration is that it enables decoupled, stratified recovery of heat with each individual PPW screened at the different depth intervals in the aquifer. Using three separate discharge channels for the recovered heat with each PPW aboveground will avoid mixing between hot water that is abstracted at the upper part of the aquifer with cooler water at the bottom of the aquifer. In Fig. 6a is shown that this decoupled heat

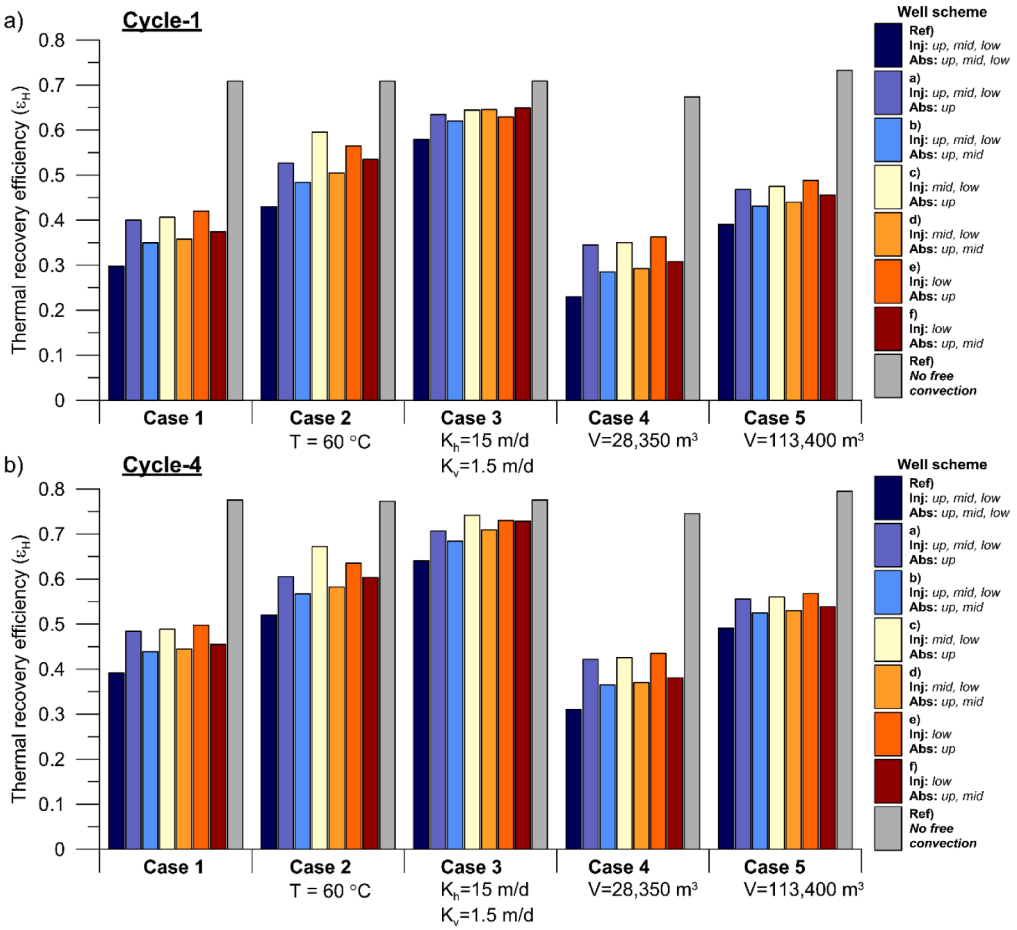

Fig. 5. Calculated thermal recovery efficiency for all cases and well scheme configurations of **a)** cycle-1 and **b)** cycle-4.

Table 5
Summary of the thermal recovery efficiency for the best performing MPPW schemes in cycle-1 and its relative difference with conventional, fully screened HT-ATES and the theoretical case with no free thermal convection.

	Well operation scheme	Inj. PPWs	Abs. PPWs	ε_H	Thermal recovery efficiency difference ($\Delta\varepsilon_H$)	
					Conventional HT-ATES	*Theoretical case (nfc)*
Case 1 *Base case*	1.e	*lower*	*upper*	0.42	+0.12	−0.29
Case 2 *T = 60 °C*	2.c	*middle, lower*	*upper*	0.59	+0.16	−0.11
Case 3 *K_h=15 m/d*	3.f	*lower*	*upper, middle*	0.65	+0.07	−0.06
Case 4 *V = 28,350 m³*	4.e	*lower*	*upper,*	0.36	+0.13	−0.31
Case 5 *V = 113,400 m³*	5.e	*lower*	*upper*	0.48	+0.09	−0.24

recovery resulted in production temperatures ranging from 62 to 46 °C in the upper PPW, while production temperatures ranging from 37 to 22 °C are recovered in the lower PPW. This means that in a full recovery cycle a total amount of 2594 GJ is recovered in the upper PPW, while this is only 305 GJ in the lower PPW.

Using a cut-off temperature of 40 °C for the HT-ATES system in Case 1.*ref*, usable heat can only be abstracted in the first 20 days if the temperatures of all PPWs are mixed, resulting in a total amount of only 1171 GJ (Table 6). However, decoupled recovery of heat during fully screened recovery under the conditions in Case 1.*ref* prolongs heat recovery above cut-off temperature in the upper PPW up to 90 days, while in the middle PPW recovery lasts 10 days (Fig. 6a). Hence, the recovered usable heat is increased by a factor of 2.4 (2780 GJ) using three separate discharge channels for each PPW. Such improvement is also obtained for the cases with a lower temperature (Case 2), a lower injection volume (Case 4) and a higher injection volume (Case 5). Only for Case 3 no improvement is found with the method of decoupled recovery. In this case the average production temperature of all PPWs remains above cut-off temperature for the entire recovery period of 90 days, recovering the total volume of 56,700 m^3. During decoupled recovery, the production temperatures in the middle and lower PPW are above cut-off temperature for only 85 and 40 days respectively (Fig. 6c). This results in a total abstracted volume of only 45,150 m^3. Hence, only 7382 GJ of heat above cut-off temperature is recovered instead of the 10,502 GJ if the recovered heat from all PPWs is mixed (Table 6).

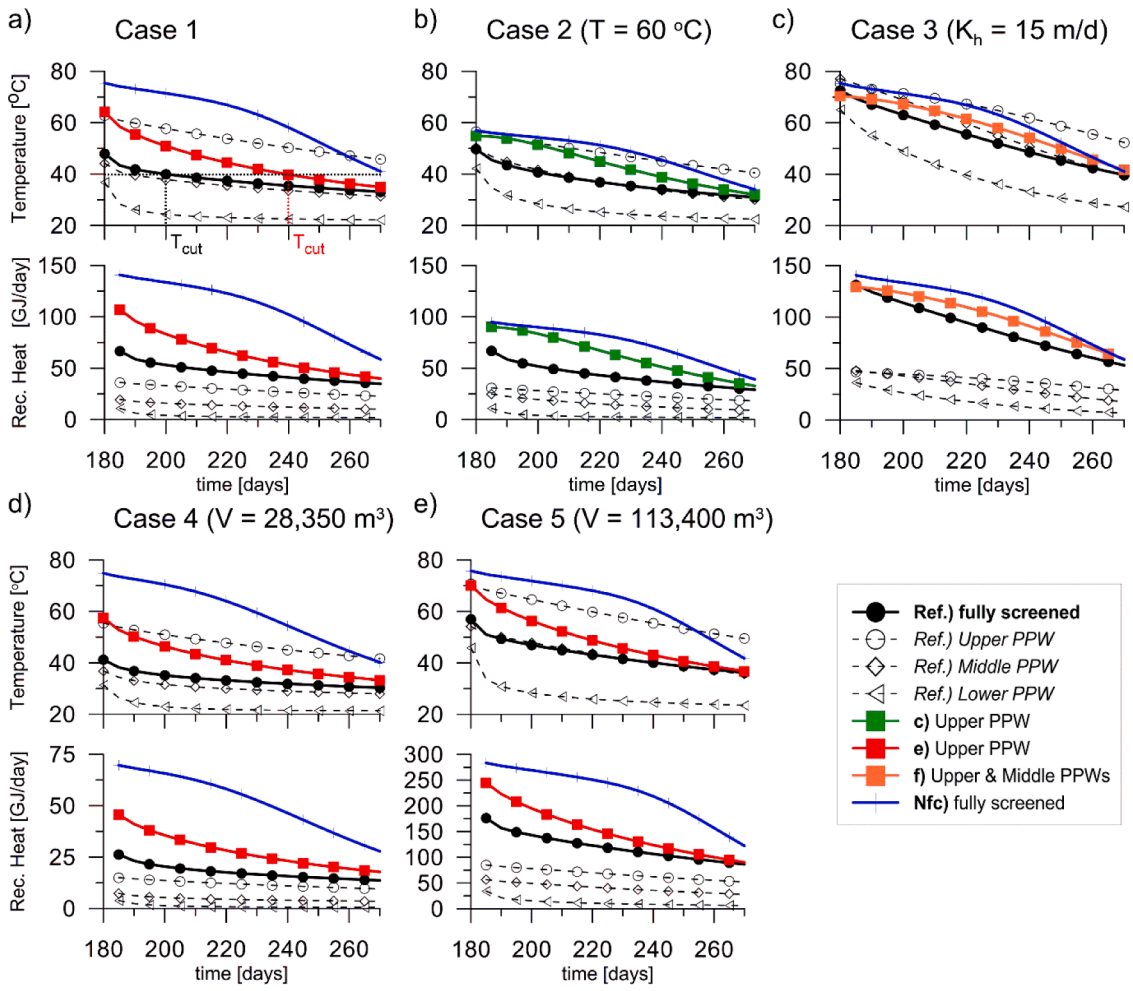

Fig. 6. Production temperature and recovered heat per day over time for cycle-1. For all cases the results for conventional HT-ATES, for the scenario with the best performing MPPW scheme that resulted in the highest recovery efficiency, and for the theoretical scenario with no free thermal convection are shown. Note that the black dashed lines represent the resulting production temperatures and recovered heat per day in the individual *upper, middle* and *lower* PPWs, while operating conventional HT-ATES with fully screened injection and abstraction in the aquifer.

Table 6
The duration of the recovery and the total amount of recoverable, usable heat at a cut-off temperature of 40 °C for the simulated cases in the sensitivity analysis for cycle-1.

	Conventional, fully screened HT-ATES		Best performing MPPW scheme			Decoupled temperature recovery with MPPW		
	time [days]	Recovered usable heat [GJ]	scheme	time [days]	Recovered usable heat [GJ]	PPW	time [days]	Recovered usable heat [GJ]
Case 1	**20**	**1171**	***e)***	**60**	**4461**	*Up.*	90	2594
Base case						*Mid.*	10	186
						Low.	0	0
						Total	–	**2780**
Case 2	**20**	**1160**	***c)***	**55**	**4104**	*Up.*	90	2172
T = 60 °C						*Mid.*	25	531
						Low.	5	55
						Total	–	**2758**
Case 3	**90**	**8014**	***f)***	**90**	**10,502**	*Up.*	90	3501
K_h=15 m/d						*Mid.*	85	2843
						Low.	40	1038
						Total	–	**7382**
Case 4	**5**	**263**	***e)***	**45**	**3102**	*Up.*	90	2148
V = 28,350 m^3						*Mid.*	0	0
						Low.	0	0
						Total	–	**2148**
Case 5	**60**	**3987**	***e)***	**70**	**5777**	*Up.*	90	3037
V = 113,400 m^3						*Mid.*	60	1355
						Low.	5	86
						Total	–	**4478**

3.3. Effect of MPPWs in heterogeneous aquifers

The best performing MPPW scheme in the *base case* with injection in the lower PPW and abstraction in the upper PPW is also tested under heterogeneous aquifer conditions. This results in different improvements of thermal recovery efficiency compared to equivalent homogeneous anisotropic conditions (Fig. 7 and Table 7). Under homogeneous anisotropic aquifer conditions, free thermal convection results in clear thermal front tilting during infiltration and storage over the entire thickness of the aquifer (Fig. 4a-b). However, under heterogeneous conditions, this thermal front tilting is not observed and thermal breakthrough in the aquifer is determined by preferential flow in the high-permeability layers and the restriction of free thermal convection by the various layers in the aquifer (Fig. 8 and 9).

In the heterogeneous layered aquifer with a high-permeability layer of 75 m/d at the top and bottom and a low-permeability layer of 10 m/d in the middle of the aquifer (Case H.1), the thermal recovery efficiency improved from 0.33 with fully screened recovery to 0.47 with the tested well operation scheme for cycle-1. Due to the low-permeability layer in the middle of aquifer H.1, upward transport of heat by free thermal convection from the lower part to the upper part of the aquifer is significantly hampered in the injection and storage stage. Fig. 8d shows that a significant amount of heat accumulates in the lower part of the aquifer below the low-permeability layer after the injection stage (90 days), while this does not occur under equivalent homogeneous conditions. Due to restricted upward flow in this low-permeability layer, more heat is stored in the upper and middle part of the aquifer after 180 days of storage. Hence, with targeted recovery in only the upper part of the

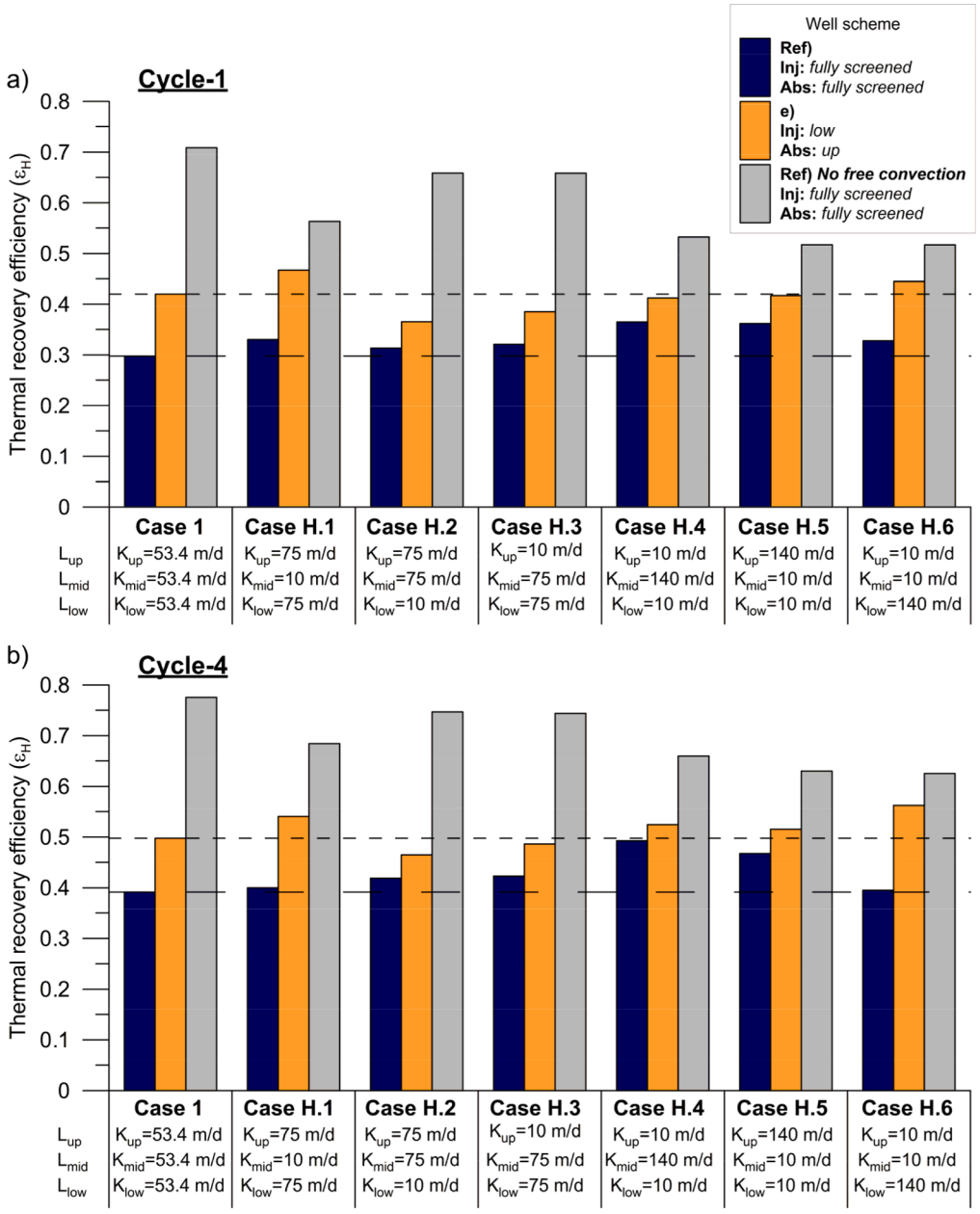

Fig. 7. Calculated thermal recovery efficiency for all heterogeneous cases and the given well operation scheme **a)** of cycle-1 and **b)** cycle-4.

Table 7
Calculated well head for infiltration of hot water of 80 °C for the simulated heterogeneous aquifer scenario's and the relative difference in thermal recovery efficiency between the simulated MPPW setup and conventional, fully screened HT-ATES, as well as the difference with the theoretical case of no free thermal convection.

Well scheme	e) *lower PPW*							ref) *all PPWs*
Case	1	H1	H2	H3	H4	H5	H6	1
Infiltration well head Δh_{PPW} [m]	2.3	2.1	5.3	2.1	5.1	5.3	1.9	1.4
Conventional HT-ATES: $\Delta\varepsilon_H$ [-]	+0.12	+0.14	+0.05	+0.06	+0.05	+0.06	+0.11	–
Theoretical case: $\Delta\varepsilon_H$ [-]	−0.29	−0.10	−0.29	−0.27	−0.12	−0.10	−0.07	–

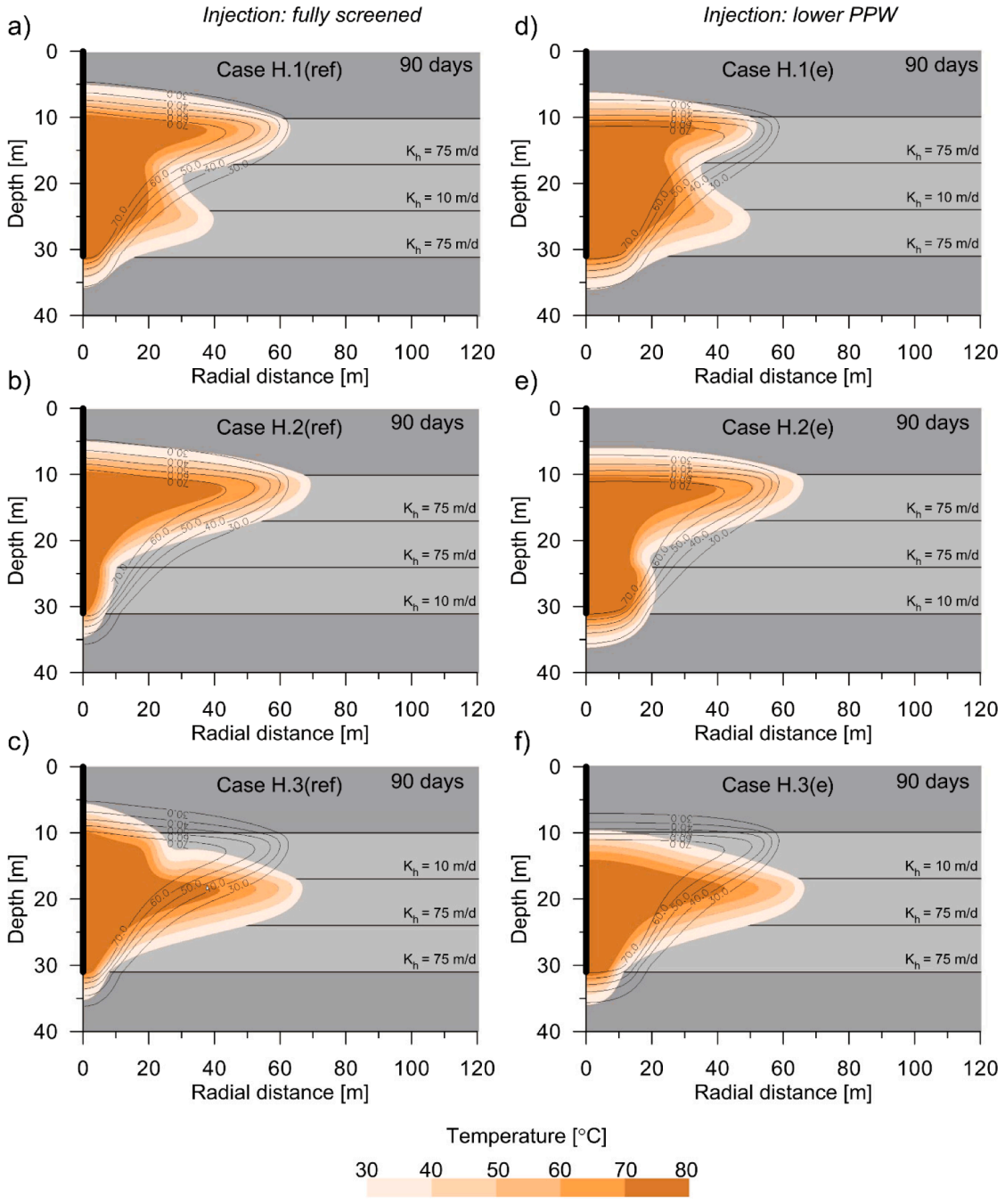

Fig. 8. The temperature distribution contour lines in the aquifer after 90 days during injection in the upper, middle and lower PPWs (well scheme *ref.*) for **a)** Case H.1, **b)** Case H.2 and **c)** Case H.3. Similarly, the temperature distribution contour lines in the aquifer are shown for an equivalent scenario with injection in only the lower PPW (well scheme for **d)** Case H.1, **e)** Case H.2 and **f)** Case H.3. The black contour lines indicate the temperature distribution calculated for equivalent homogeneous anisotropic aquifer conditions (Case 1).

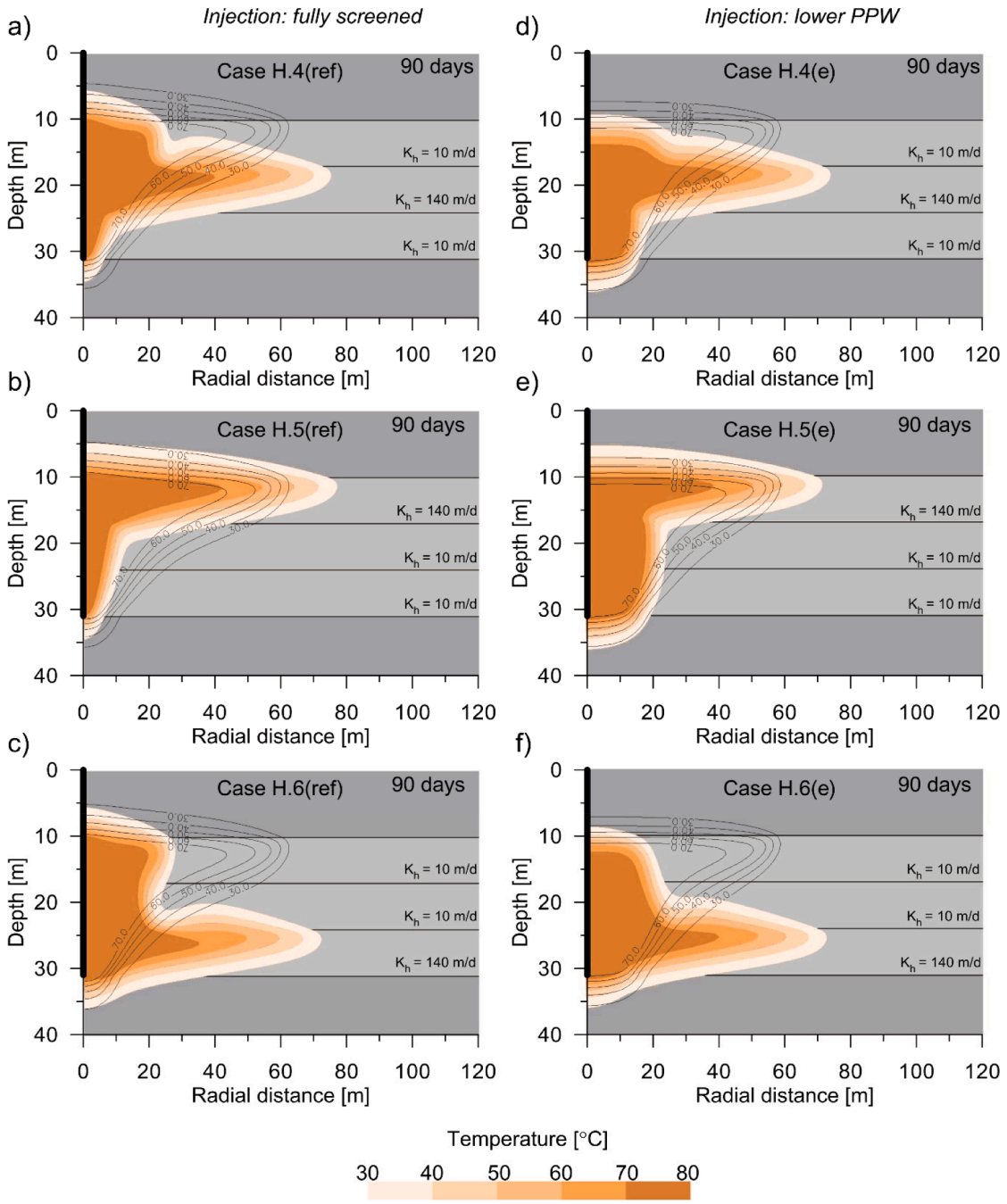

Fig. 9. The temperature distribution contour lines in the aquifer after 90 days during injection in the upper, middle and lower PPWs (well scheme *ref.*) for **a)** Case H.4, **b)** Case H.5 and **c)** Case H6. Similarly, the temperature distribution contour lines in the aquifer are shown for an equivalent scenario with injection in only the lower PPW (well scheme for **d)** Case H.4, **e)** Case H.5 and **f)** Case H.6. The black contour lines indicate the temperature distribution calculated for equivalent homogeneous anisotropic aquifer conditions (Case 1).

aquifer, where most of the heat is accumulated, a large thermal recovery efficiency improvement is obtained ($\Delta\varepsilon_H = +0.14$).

This is very close to the theoretical case with no free convection with a difference ($\Delta\varepsilon_H$) of only -0.10, while under equivalent homogeneous anisotropic conditions (Case 1.*e*) the difference is -0.29. Note that under theoretical conditions with no free thermal convection, the highest recovery efficiencies are obtained for the scenarios with the smallest contact area between the hot water volume and cooler ambient groundwater (Fig. 7). In these cases heat loss by thermal conduction is low. Hence, distinct heterogeneous layering in the aquifer, such as in aquifer H.1, results in a more irregularly-shaped storage volume in the aquifer and significantly more heat loss by thermal conduction. This results in theoretical recovery efficiency of only 0.56 for aquifer H.1 while in an equivalent homogeneous anisotropic aquifer the theoretical recovery efficiency is 0.71 for cycle-1. Similar theoretical thermal recovery efficiencies are found for aquifers H.4–6, resulting also in smaller thermal recovery efficiency differences between the theoretical scenarios and the tested MPPW schemes (Fig. 7 and Table 7).

Only a small improvement in thermal recovery efficiency ($\Delta\varepsilon_H$ of approximately +0.05) with injection in the lower PPW and abstraction in the upper PPW is obtained compared to fully screened well operation in the aquifers H.2 and H.3 for cycle-1. In this case enhanced free thermal convection is observed in the 14 m-thick high-permeability layer (K_h=75 m/d and K_v=25 m/d) of the aquifer, while flow in the low permeability layer is restricted (Fig. 8b,c,e,f). In aquifer H.2, a significant amount of heat remains stored in the low permeability layer, which will not be recovered by the upper PPW. Moreover, more heat is stored in the upper part of the aquifer resulting in significant heat loss by thermal conduction due to a large contact surface area between the heated aquifer and the cooler overlying confining layer (Fig. 8d). This effect of heat loss by thermal conduction into the overlying confining layers is significantly smaller for aquifer H.3, where heat accumulates in the middle part of the aquifer due to thermal front tilting below the low-permeability layer after 90 days of injection (Fig. 8f). Recovery in the upper low-permeability layer will not be able to abstract the accumulated heat in the middle of the aquifer at a large radial distance.

For the scenarios with a high permeability layer of 140 m/d, the preferential accumulation of heat is even more distinct (Fig. 9). In aquifer H.6 a significant improvement in thermal recovery efficiency is obtained compared to fully screened well operation ($\Delta\varepsilon_H = +0.11$), which is very close to the theoretical case (Table 7). Upward heat transport by free thermal convection through the low-permeability layer of 14 m thickness is slow and after approximately 90 days it reaches the top of the aquifer (Fig. 9f). Hence, no thermal front tilting in the low-permeability is observed, while this is already the case during fully screened well operation (Fig. 9c). Due to ongoing heat transport from the high-permeability layer at the bottom to the upper part of the aquifer after the recovery stage, and also in the subsequent recovery cycles, the improvement with the tested well operation scheme becomes even larger for cycle-4 ($\Delta\varepsilon_H = +0.17$).

The improvement in thermal recovery efficiency by infiltration in only the *lower* PPW, as well as abstraction in only the upper PPW, comes at the price of higher pumping costs due to additional head losses by partial penetration. Infiltration in all PPWs with a conventional, fully screened HT-ATES system requires a well head of approximately 1.4 m (Table 6). During infiltration and abstraction using only one PPW, forced convection occurs in both the horizontal and vertical direction. The extent of the vertical flow component around the PPW depends on the aquifer characteristics and the length of the well screen (e.g. Tügel et al., 2016; Van Lopik et al., 2021). Especially for scenarios where infiltration and abstraction occur solely in the low-permeability layers of 10 m/d, the required well heads are high. For example, the required well head to infiltrate hot water at a temperature of 80 °C in the lower *PPW* is approximately 5.1–5.3 m for aquifers H2, H4 and H5, while this is only 2.3 m under homogeneous aquifer conditions (Table 7).

4. Discussion

4.1. MPPW potential to mitigate the impact of free thermal convection on HT-ATES performance

This numerical study shows that a MPPW configuration with a proper well operation scheme for injection and recovery can be used to counter the effects of heat loss by free thermal convection and increase the performance of seasonal HT-ATES systems. Especially for scenarios with a significant effect of thermal front tilting close to the well screen, MPPW configurations can be used to control the thermal front and improve the thermal recovery efficiency. Besides the overall thermal recovery efficiency, the MPPW configuration significantly improves the performance of HT-ATES systems that require a given cut-off temperature to supply the demanded usable heat (i.e. for industry applications, district heating systems and greenhouse agriculture). In the simulated scenarios with hot water storage at temperatures of 80 and 60 °C in the high-permeability aquifer (Case 1 and 2), the total amount of recovered usable heat at a cut-off temperature of 40 °C improved by a factor of 4 in the first cycle while using the best performing MPPW scheme instead of conventional, fully screened HT-ATES. In this first cycle, the recovery stages of usable heat abstraction are still relatively short with a duration of only 60 and 55 days for respectively Case 1 and 2 (Table 6). Note that in reality abstraction will be stopped after cut-off temperature is reached. This will result in a larger amount of accumulated heat in the aquifer for each subsequent recovery cycle and thus prolonged recovery until the cut-off temperature is reached for the upcoming recovery cycles.

Moreover, a MPPW configuration also enables decoupled recovery of heat at specific depths in the aquifer, while with a fully-penetrating well only one quality of heat can be abstracted. In practice, heat supply from a HT-ATES system can be coupled to multiple energy-systems with each its own heat quality demand. Decoupling thermal recovery with MPPWs can prolong recovery of high quality heat above a required cut-off temperature in the upper part of the aquifer, while lower heat quality from the lower part of the aquifer can be used for different purposes. For example, the HT-ATES system of Case 1.*ref* could provide high quality heat (production temperatures higher than 40 ^{0}C) for 90 days with the *upper* PPW, while recovery of low quality heat from the *middle* or *lower* PPW heat can be decoupled and provided to another heat distribution system (Fig. 6a).

In the simulated scenarios, only seasonal HT-ATES is considered with equal periods of 90 days of injection, storage and abstraction. In HT-ATES systems that suffer from severe free thermal convection, such as storage in high-permeability aquifers, and storage at large temperature contrasts between hot injection water and cold ambient groundwater, shortening the period between injection and recovery might be an option (e.g. Sheldon et al., 2021). However, in many cases leveling the annual mismatch between heat supply and demand won't be feasible with HT-ATES systems operating at such short recovery cycles. The implementation of a MPPW configuration can only help to prolong the time between injection and recovery to a limited extent for scenarios that suffer from severe free thermal convection. If the injection and storage stages during seasonal HT-ATES are too long, a MPPW configuration fails to counter the effects of thermal front tilting successfully before recovery starts. For example, in Case 1.*e* the hot water volume already reaches the top of the aquifer after 45 days of injection in the lower PPW. The prolonged period between injection and recovery (180 days) will inevitably result in more accumulation of hot injection water in the upper part of the aquifer and considerable heat loss to the overlying confining layer. Naturally, the vertical transport will take longer in thicker aquifers than the ones investigated in this study under similar buoyancy components, and will reduce the heat loss to some extent. For HT-ATES systems that could operate at relative short recovery cycles due to a more variable heat surplus and demand over the year (i.e. for industry purposes), a MPPW configuration can help to improve the production temperatures over time and the overall thermal recovery efficiency drastically.

Recirculation of accumulated hot water in the top of the aquifer by reinjection in the lower part of the aquifer during the storage stage might be considered with the MPPW configuration to counter the effects of free thermal convection, if shortening of the recovery cycles is not an option. In practice, this will require extensive analysis for specific HT-ATES designs to predict optimal thermal front stabilization at a minimum of pumping costs using this principle of vertically differentiated simultaneous abstraction and re-injection of hot water.

If heat supply and demand is strictly seasonal, hot water storage at moderate temperature differences and significant reduction of thermal recovery efficiency by free thermal convection can benefit from a MPPW configuration with the proposed well operation schemes. The results show that storage at a temperature difference (ΔT) of 40 °C with the best performing MPPW scheme the thermal recovery efficiencies are much closer to the theoretical case of no free thermal convection (Case 2.*nfc*) compared to *base case* ($\Delta T = 60$ °C, Case 1). This difference in $\Delta\varepsilon_H$ is only −0.11 (Table 5). Similar improvements of the thermal recovery efficiency under the same aquifer and storage characteristics were found in the study of Van Lopik et al. (2016). In this study optimization of the thermal recovery efficiency by using density difference compensation for the hot injection water by increasing its salinity was tested. With the density difference compensation, the thermal recovery efficiency difference ($\Delta\varepsilon_H$) is −0.05 at a temperature difference (ΔT) of 40 °C. However, as described above, for scenarios with significant free thermal convection the differences remain large. For comparison, in the *base case* (Case 1 at $\Delta T = 60$ °C) the calculated difference ($\Delta\varepsilon_H$) in this study is −0.29, while in the study of Van Lopik et al. (2016) a calculated difference ($\Delta\varepsilon_H$) of only −0.07 was obtained.

4.2. Application of a monitoring scheme to track thermal distribution in the aquifer during HT-ATES operation

Obtaining a detailed and reliable overview of the hydrogeological conditions might be a challenging and costly procedure. The lack of such data makes it difficult to predict the thermal distribution in the aquifer and, consequently, the thermal interface between the injected hot water and cold ambient groundwater over the entire aquifer thickness during HT-ATES operation. This holds especially for a MPPW configuration which allows for injection and abstraction in different parts of the aquifer. Hence, accurate monitoring of the temperature distribution in the aquifer at different radii from the well during injection and abstraction with a MPPW configuration is essential. A selection of proper monitoring distances from the HT-ATES well will allow spatial and temporal tracking of the hot water volume and will prevent relying heavily on numerical predictions during well operation. This will be useful to provide insight in the quality of heat around the individual PPWs over time and to predict which production temperatures can be expected over time during recovery.

In practice, the temperature distribution can be monitored over the entire thickness of the aquifer during HT-ATES. In the HT-ATES field pilot of Bloemendal et al. (2019), distributed temperature sensing (DTS) with optical fibres to monitor the temperature distribution over aquifer depth was used. A similar setup is chosen to investigate if the thermal front can be monitored properly for the simulated scenarios in this study.

For the *base case*, the temperature distribution in the aquifer is monitored at distances of 5, 10 and 25, which lie within the maximum average thermal radius of influence of 38,75 m (see Table 2). Fig. 10 shows that tilting of the thermal front can be tracked at radial distances of 5, 10 and 25 m for conventional, fully screened HT-ATES. The tem-

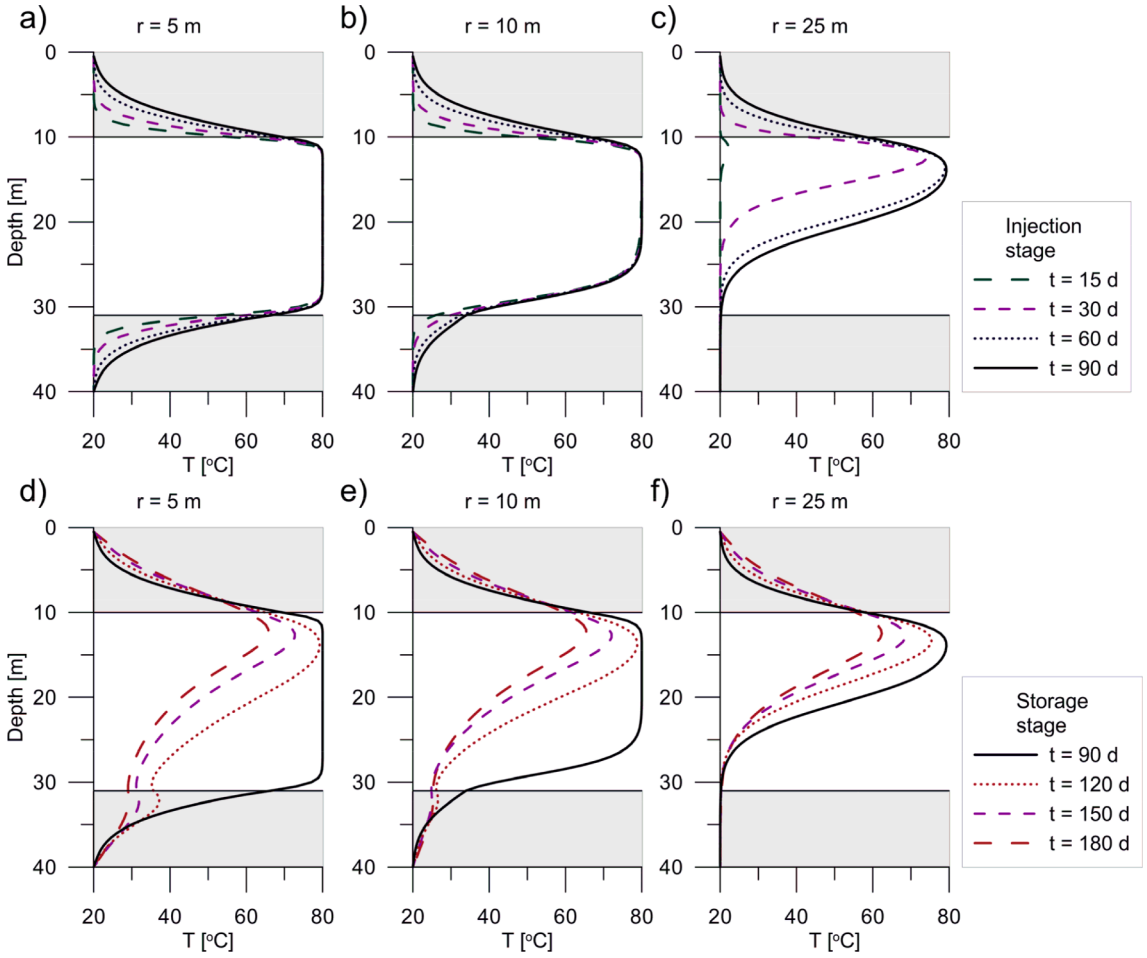

Fig. 10. The temperature over depth over time at different times for conventional, fully screened HT-ATES (Case 1.*ref*) at a radial distance of **a)** 5, **b)** 10 and **c)** 25 m from the HT-ATES well during injection. Similarly, the temperature over depth at **d)** 5, **e)** 10 and **f)** 25 m from the HT-ATES well during storage is shown.

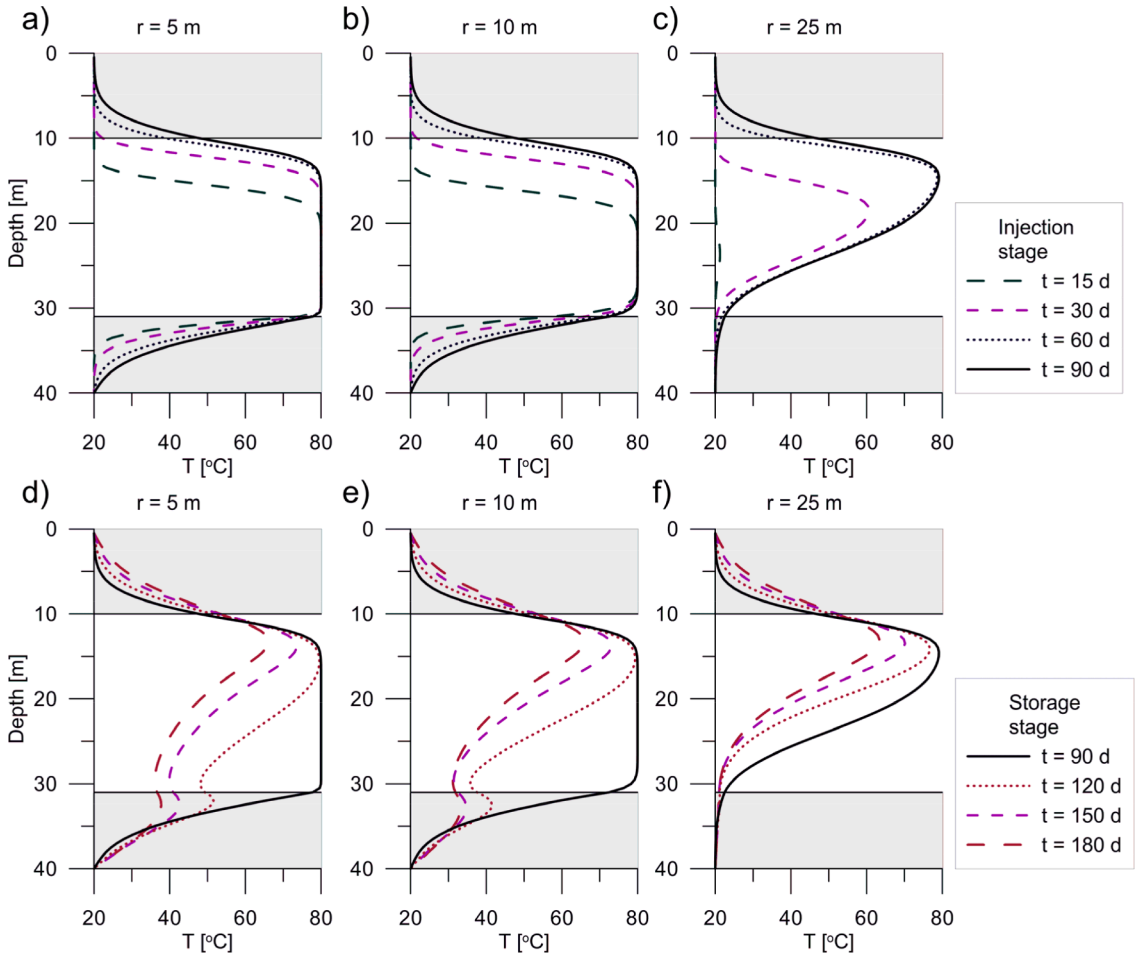

Fig. 11. The temperature over depth at different times for HT-ATES with injection in the lower PPW (Case 1.*e*) at a radial distance of **a)** 5, **b)** 10 and **c)** 25 m from the HT-ATES well during injection. Similarly, the temperature over depth at **d)** 5, **e)** 10 and **f)** 25 m from the HT-ATES well during storage is shown.

perature contour of 50 °C at a radius of 10 and 25 m is at a depth of 28 m (Fig. 10b) and 15.5 m (Fig. 10c), respectively after 30 days. Based on these results the tilting angle is 27°. At the end of the injection stage, the depth of the temperature contour of 50 °C is respectively 29 m (Fig. 10b) and 21.3 m (Fig. 10c) at a radius of 10 and 25 m, resulting in a tilting angle of approximately 63°. In this case, extrapolation of the data can provide an estimate of the thermal front in this anisotropic, homogeneous aquifer. However, a similar monitoring setup fails to estimate the location of the thermal front during injection of hot water in only the *lower* PPW (Cases 1.*e*) during the injection stage. Due to the more compact hot water volume at the end of the injection stage (see Fig. 4d), the temperature contour of 50 °C is only monitored at a radius of 25 m in the middle of the aquifer (Fig. 11c). In the *base case*, monitoring at radial distances between 25 and 40 m will provide better data to track the thermal front for both well configurations in the injection stage (see Fig. 12a and 13a). However, the narrowing of the thermal front at *lower* PPW depth in the storage stage due to ongoing free thermal convection is perfectly tracked with the suggested monitoring at radii of 5 and 10 m for both Case 1.*ref* (Fig. 10d-f) and Case 1.*e* (Fig. 11d-f).

Tracking the thermal distribution over time with a proper monitoring system during operation of the HT-ATES system could also provide useful information on preferential heat transport due to aquifer heterogeneity and its associated accumulation of heat in the aquifer (Fig. 12 and 13). For homogeneous anisotropic aquifer conditions it is easier to estimate the temperature front based on a few monitoring location, since free thermal convection results in clear thermal front tiling and cone-shaped storage of heat in the aquifer (Fig. 3). However, in aquifers with distinct heterogeneous layering, no clear tilting of the thermal front will be observed. Figs. 12 and 13 show that preferential heat transport by forced and free convection in the high-permeability layers can be easily tracked at the monitoring distances of 25 and 40 m. In practice, it will be advisable to select multiple monitoring locations that will enable tracking both the temperature front in the near well vicinity, and the temperature front at larger radial distances beyond the theoretical maximum average thermal radius of influence for a scenario with no free thermal convection (Eq. (6)), to capture the impact of both free thermal convection, as well as preferential heat transport in high-permeability layers on the thermal front.

For highly variable and unpredictable injection and recovery duration and volumetric flow rates over time, a proper monitoring scheme can be used to control HT-ATES operation. Monitoring data on the accumulation of heat over the entire thickness of the aquifer at given radial distances could be used to control well operation for each PPW during the injection and recovery stage to stabilize the hot water volume and minimize the effects of free thermal convection over time. The existing knowledge in the field of aquifer storage and recovery (ASR) could also be applied in HT-ATES systems. In ASR systems the selection of an efficient injection and abstraction well operation scheme in a

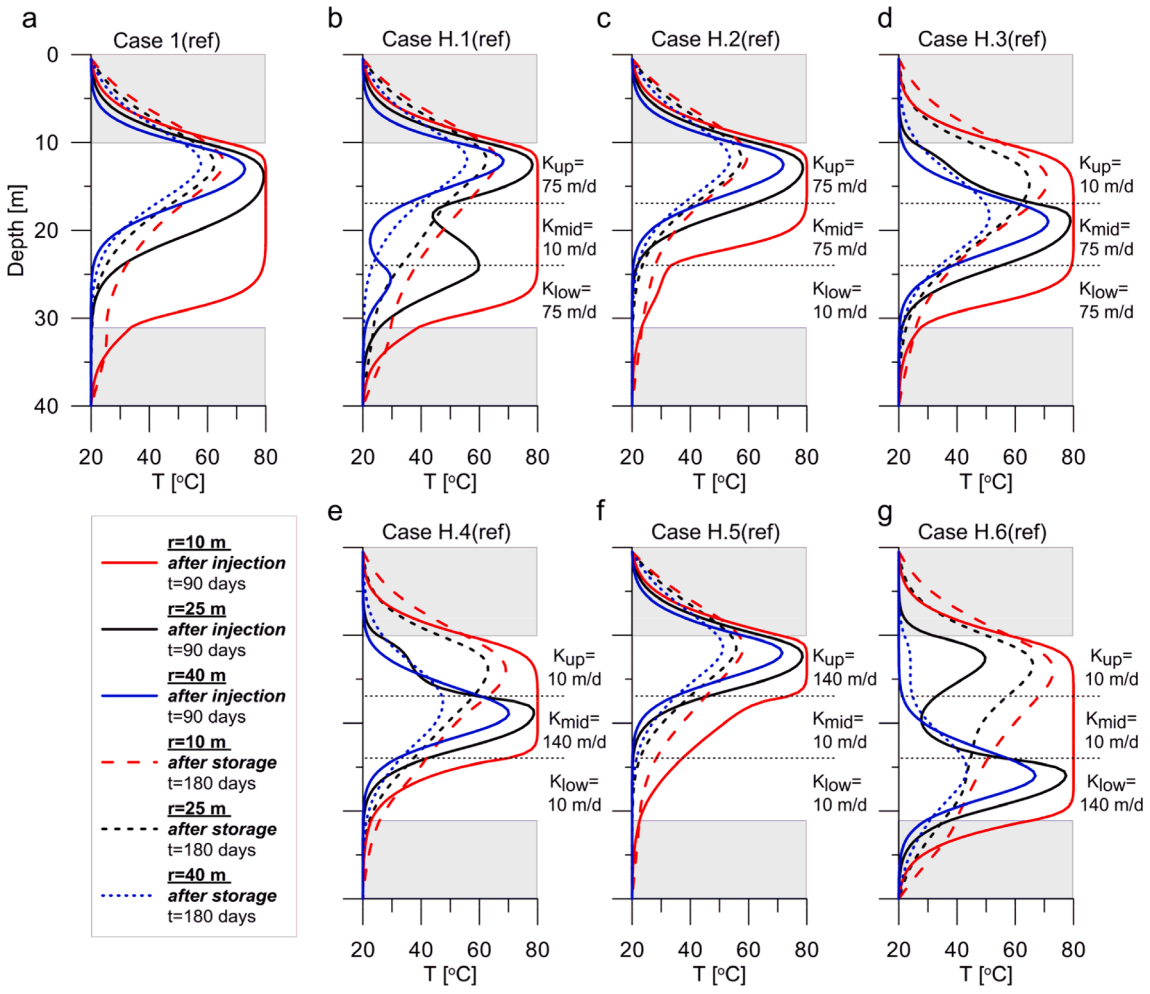

Fig. 12. The temperature over depth after 90 (injection) and 180 days (storage) for conventional, fully screened HT-ATES (well scheme *ref.*) in the heterogeneous-layered aquifers (H.1–6) and the equivalent homogeneous anisotropic aquifer (Case 1) at radial distances of 10, 25 and 40 m from the well.

MPPW setup is successfully used to maintain a stable fresh water volume and to actively limit the mixing potential in brackish aquifers during fresh water storage (Zuurbier et al., 2014; Witt et al., 2021).

4.3. *Well design of the MPPWs to further enhance performance*

To date, most conceptual models for seasonal HT-ATES account for homogeneous anisotropic aquifer conditions to calculate the thermal recovery efficiency and the resulting thermal front tilting during injection and storage (e.g. Schout et al., 2014; Van Lopik et al., 2016; Sheldon et al., 2021). However, in nature, most aquifers are heterogeneous to varying extents. In these cases oversimplification of the aquifer characteristics might cause wrong predictions of the thermal distribution in the aquifer and thermal recovery efficiencies (see Fig. 7-9). This already holds for conventional, fully screened HT-ATES, but is specifically important for the planning of proper MPPW configurations. Vertical variability in the aquifer permeability largely determines optimal well placement and well dimensions of the PPWs. In natural aquifers with distinct heterogeneous layering the preferential heat transport by both forced and free convection is more complex, and the preferential layers for injection and recovery can significantly differ from an equivalent homogeneous anisotropic aquifer.

For example, in Case H.2 infiltration in the lower PPW and abstraction in the PPW screened in the upper low permeability layer (K_h = 10 m/d) resulted in a low thermal recovery efficiency of only 0.37. Fig. 13d shows that a large amount of heat is still stored in the middle, high permeability layer at radial distances of 25 and 40 m after 180 days of storage. Hence, abstraction with this well scheme will not be able to recover the accumulated heat in the middle of the aquifer. In such case, based on the temperature distribution in the aquifer, abstraction in the middle of the aquifer might be considered to improve the thermal recovery efficiency. This enables recovery of the accumulated heat at larger radial distances in the middle part of the aquifer. Besides heterogeneous layering in an aquifer, also screening injection PPWs below small lower-permeability lenses or layers could already hamper forced and free thermal convection to the overlying part of the aquifer and reduce the overall efficiency of a MPPW configuration significantly.

For determining proper well dimensions of each PPW in a heterogeneous aquifer, the implications for well hydraulics, risks of additional head loss by potential well clogging, as well as associated pumping costs need to be assessed while considering a MPPW configuration (e.g. Houben, 2015; Van Lopik et al., 2021). Screening PPWs in low-permeability layers comes at a price of higher well heads and pumping costs (Table 7) and might result in higher clogging risks due to deep-bed filtration of fines in finer sand layers. Despite significant improvement in thermal recovery efficiency with a given MPPW configuration by targeting such layers, see for example Case H.6 (Table 7), such issues might nullify the gain in thermal recovery efficiency and hamper the feasibility of the proposed MPPW operation scheme Figs. 12 and 13.

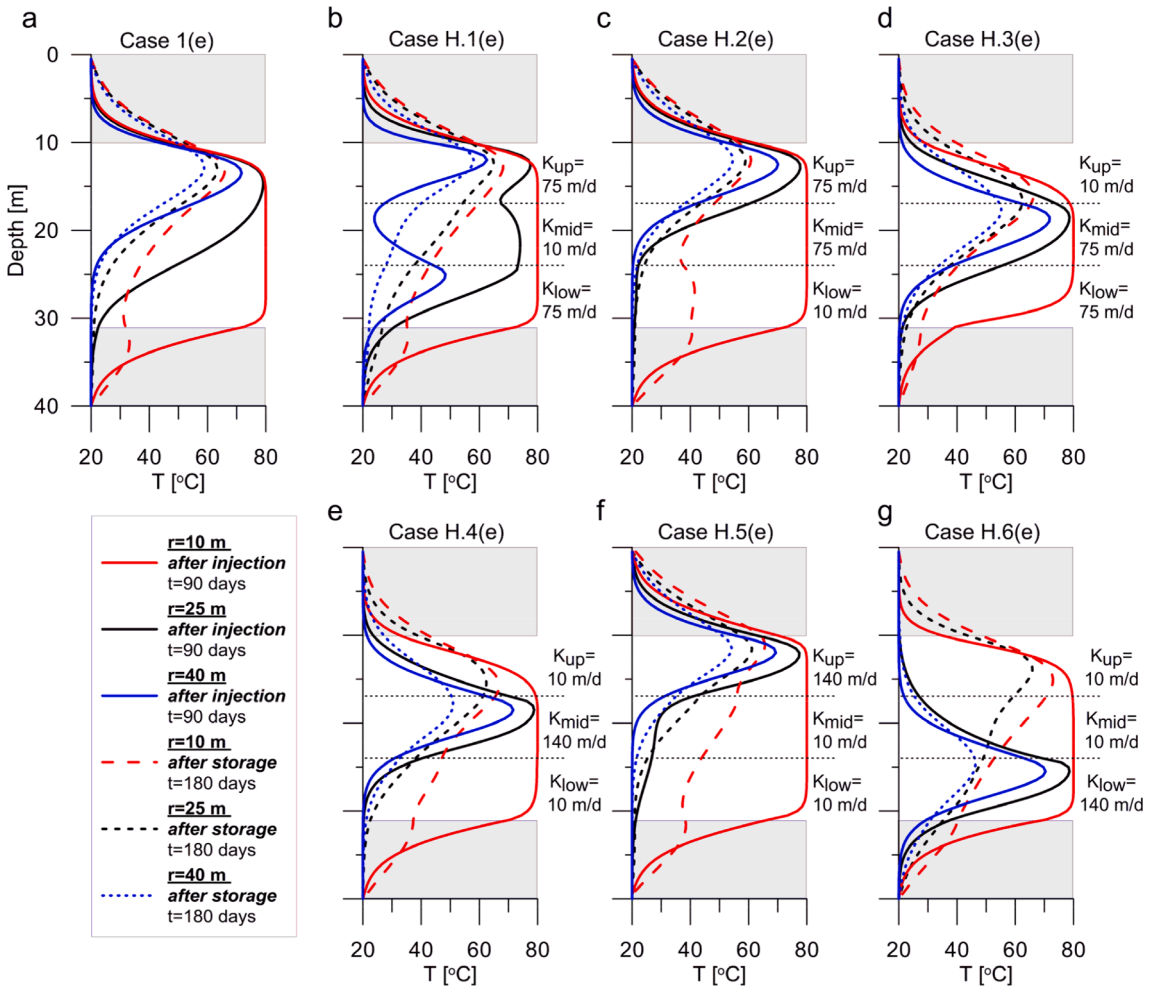

Fig. 13. The temperature over depth after 90 (injection) and 180 days (storage) for HT-ATES with injection in the lower PPW (well scheme *e*) in the heterogeneous-layered aquifers (H.1–6) and the equivalent homogeneous anisotropic aquifer (Case 1) at radial distances of 10, 25 and 40 m from the well.

5. Conclusions

A MPPW configuration has the potential to reduce the impact of free thermal convection and improve the thermal recovery efficiency in HT-ATES systems. If the effects of free thermal convection on the thermal front of the hot water volume occurs relatively close to the HT-ATES well, targeted injection in lower parts and recovery in the upper parts of the aquifer with a MPPW configuration enables significant improvement of the thermal recovery efficiency. For example, the effect of free thermal convection is countered successfully with the MPPW configuration at moderate storage temperatures of 60 °C. In a high-permeability aquifer (K_h=53.4 m/d and K_v=7.7 m/d), the thermal recovery efficiency with the best performing MPPW scheme was improved from 0.43 to 0.59 in cycle.1. This is close to the theoretical scenario of no free thermal convection with a difference ($\Delta\varepsilon_H$) of only −0.11. At a higher storage temperature of 80 °C during seasonal HT-ATES, stronger free thermal convection results in a larger difference between the thermal recovery efficiency of the scenario with best performing MPPW scheme and the theoretical scenario considering no free convection remains large ($\Delta\varepsilon_H$ = −0.29).

Moreover, HT-ATES systems with MPPW-configurations have great potential if recovered heat needs to be above a certain cut-off temperature. The best performing MPPW schemes significantly prolong the recovery of usable heat above a cut-off temperature of 40 °C during hot water storage at temperatures of 60 and 80 °C in a high-permeability aquifer. The total amount of recovered usable heat was improved by a factor of 4 compared to fully screened HT-ATES operation. The use of a MPPW-configuration instead of a fully-penetrating well can also be helpful to enable decoupled, stratified recovery of heat with individual PPWs screened at different depths in the aquifer. If usable heat above a certain cut-off temperature is required, decoupling of high quality heat and low quality heat can be done easily with the PPWs.

Investigation of the full-potential of MPPWs in order to optimize HT-ATES systems should take into account aquifer heterogeneity. Simplification of the aquifer characteristics might cause wrong estimates of the temperature distribution in the aquifer and the thermal recovery efficiency. This could lead to selection of poor well designs and less favourable well operation schemes during injection and recovery. It is highly advisable to apply accurate monitoring of the temperature distribution in the aquifer at different radii from the well during injection and abstraction with a MPPW configuration. This is essential for spatial and temporal tracking of the hot water volume in the aquifer, and can be used to predict which production temperatures can be expected over time.

CRediT authorship contribution statement

J.H. van Lopik: Writing – original draft, Investigation, Conceptualization, Methodology, Validation. **N. Hartog:** Writing – review & editing, Supervision, Conceptualization. **R.J. Schotting:** Writing – review & editing, Supervision, Funding acquisition.

Declaration of Competing Interest

The authors declare no conflict of interest.

Data Availability

Data is available within the article.

Acknowledgements

This study was supported by the foundations STW (Foundation for Technical Sciences) and O2DIT (Foundation for Research and Development of Sustainable Infiltration Techniques).

References

Alva, G., Lin, Y., Fang, G., 2018. An overview of thermal energy storage systems. Energy 144, 341–378.
Bloemendal, M., Olsthoorn, T., van der Ven, F., 2015. Combining climatic and geo-hydrological preconditions as a method to determine world potential for aquifer thermal energy storage. Sci. Total Env. 538, 621–633.
Bloemendal, M., Hartog, N., 2018. Analysis of the impact of storage conditions on the thermal recovery efficiency of low-temperature ATES systems. Geothermics 71, 306–319.
Bloemendal, M., Beernink, S., Hartog, N., van Meurs, B., 2019. Transforming ATES to HT-ATES, Insight from Dutch pilot Project. European Geothermal Congress 2019 the Netherlands, The Hague, 11-14 June 2019.
Buscheck, T.A., Doughty, C., Tsang, C.F., 1983. Prediction and analysis of a field experiment on a multi-layered aquifer thermal energy storage system with strong buoyancy flow. Water Resour. Res. 19 (5), 1307–1315.
Collignon, M., Klemetsdal, Ø.S., Møyner, O., Alcanié, M., Rindali, A.P., Nilsen, H., Lupi, M., 2020. Evaluating thermal losses and storage capacity in high-temperature aquifer thermal energy storage (HT-ATES) systems with well operating limits: insights from a study-case in the Greater Geneva Basin, Switzerland. Geothermics 85, 10773.
Dinçer, I., Rosen, M.A., 2021. Thermal Energy storage, Systems and Applications, 3thd ed. Wiley, Hoboken, NJ.
Doughty, C., Hellström, G., Tsang, C.F., Claesson, J., 1982. A dimensionless parameter approach to the thermal behavior of an aquifer thermal energy storage system. Water Resour. Res. 18 (3), 571–587.
Fleuchaus, P., Godschalk, B., Stober, I., Blum, P., 2018. Worldwide application of aquifer thermal energy storage – a review. Renew. Sustain. Energy Rev 94, 861–876.
Fleuchaus, P., Schüppler, S., Bloemendal, M., Gugleilmetti, L., Opel, O., Blum, P., 2020. Risk analysis of High-Temperature aquifer thermal energy storage (HT-ATES). Renew. Sustain. Energy Rev 133, 110–135.
Guo, W., Langevin, C.D., 2002. User's guide to SEAWAT: a computer program for simulation of three-dimensional variable-density ground-water flow. US Geological Survey, Techniques of Water-Resources Investigations 6-A7, US Geological Survey, Reston, Virginia, USA.
Harbaugh, A.W., Banta, E.R., Hill, M.C., McDonald, M.G., 2000. MODFLOW-2000, the US Geological Survey modular ground-water models: user guide to modularization concepts and the ground-water flow process. US Geological Survey, Open-File Report 00-92.
Holstenkamp, L., Meisel, M., Neidig, P., Opel, O., Steffahn, J., Strodela, N., Lauer, J.J., Vogel, M., Degenhart, H., Michalzik, D., Schomerus, T., Schönebeck, J., Növig, T., 2017. Interdisciplinary review of medium-deep aquifer thermal energy storage in North Germany. Energy Procedia 135, 327–336.
Hellström, G., Tsang, C.F., Claesson, J., 1979. Heat Storage in aquifers: Buoyancy Flow and Thermal Stratification Problems. Institute of Technology, Lund, Sweden and as Rep. LBL-14246, Lawrence Berkeley Lab, Berkeley, CA.
Houben, G.J., 2015. Review: hydraulics of water wells—flow laws and influence of geometry. Hydrogeol. J. 23, 1633–1657.
Kabus, F., Seibt, P., 2000. Aquifer thermal energy storage for the berlin reichstag building – new seat of the German parliament. In: Proceedings of the World Geothermal Congress 2000. Kyushu, Tohoku, Japan. May 28-June 10 2000,.
Langevin, C.D., 2008. Modeling axisymmetric flow and transport. Ground Water 46 (4), 579–590.
Langevin, C.D., Thorne Jr., D.T., Dausman, A.M., Sukop, M.C., Guo, W., 2008. SEAWAT Version 4: a computer program for simulation of multi-species solute and heat transport. US Geological Surv. Tech. Meth. 6, A22. -.
Maliva, R.G., Missimer, T.M., 2010. Aquifer Storage and Recovery and Managed Aquifer Recharge Using wells: Planning, hydrogeology, Design and Operation. Schlumberger Water Services.
Molz, F.J., Melville, J.G., Güven, O., Parr, A.D., 1983b. Aquifer thermal energy storage: an attempt to counter free thermal convection. Water Resour. Res. 19 (4), 922–930.
Molz, F.J., Melville, J.G., Parr, A.D., King, D.A., Hopf, M.T., 1983a. Aquifer thermal energy storage: a well doublet experiment at increased temperatures. Water Resour. Res. 19 (1), 149–160.
Opel, O., Strodel, N., Werner, K.F., Geffken, J., Tribel, A., Ruck, W.K.L., 2017. Climate-neutral and sustainable campus Leuphana University of Lueneburg. Energy 141, 2628–2639.
Réveillère, A., Hamm, V., Lesueur, H., Cordier, E., Goblet, P., 2013. Geothermal contribution to the energy mix of a heating network when using Aquifer Thermal Energy Storage: modeling and application to the Paris basin. Geothermics 47, 69–79.
Schout, G., Drijver, B., Gutierrez-Neri, M., Schotting, R., 2014. Analysis of recovery efficiency in high-temperature aquifer thermal energy storage: a Rayleigh-based method. Hydrogeol. J. 22 (1), 281–291.
Sharqawy, M.H., Lienhard, V.J.H., Zubair, S.M., 2010. Thermophysical properties of seawater: a review of existing correlations and data. Desalinat. Water Treat 16 (1–3), 354–380. https://doi.org/10.5004/dwt.2010.1079.
Sheldon, H.A., Wilkins, A., Green, C.P., 2021. Recovery efficiency in high-temperature aquifer thermal energy storage systems. Geothermics 96, 102173.
Stricker, K., Grimmer, J., Egert, R., Bremer, J., Korzani, M.G., Schil, e., Kohl, T., 2020. The potential of depleted oil reservoirs for High- Temperature Storage Systems. Energies 13, 6510.
Tügel, F., Houben, G.J., Graf, T., 2016. How appropriate is the Thiem equation for describing groundwater flow to actual wells? Hydrogeol. J. 24 (8), 2093–2101.
Ueckert, M., Bauman, T., 2019. Hydrochemical aspects of hightemperature aquifer storage in carbonaceous aquifers: evaluation of a field study. Geotherm. Energy 7 (4).
UN., 2015. Paris Agreement - Report of the Conference of the Parties to the United.
Vandenbohede, A., Louwyck, A., Vlamynck, N., 2014. SEAWAT-based simulation of axisymmetric heat transport. Ground Water 52 (6), 908–915.
Van der Roest, E., Beernink, S., Hartog, N., van der Hoek, J.P., Bloemendal, M., 2021. Towards sustainable heat supply with decentralized multi-energy systems by integration of subsurface seasonal heat storage. Energies 14, 7958.
Van Lopik, J.H., Hartog, N., Zaadnoordijk, W.J., Cirkel, D.G., Raoof, A., 2015. Salinization in a stratified aquifer induced by heat transfer from well casings. Adv. Water Resour. 86A, 32–45.
Van Lopik, J.H., Hartog, N., Zaadnoordijk, W.J., 2016. The use of salinity contrast for density difference compensation to improve the thermal recovery efficiency in high-temperature aquifer thermal energy storage systems. Hydrogeol. J. 24 (5), 1255–1271.
Van Lopik, J.H., Sweijen, T., Hartog, N., Schotting, R.J., 2021. Contribution to head loss by partial penetration and well completion: implications for dewatering and artificial recharge wells. Hydrogeol. J. 29, 875–893.
Voss C.I., 1984. A finite-element simulation model for saturated-unsaturated, fluid-density-dependent ground-water flow with energy transport or chemically-reactive single-species solute transport. Water resources investigations report 84-4369. U.S. Geological Survey.
Winterleitner, G., Schütz, F., Wenzelaff, C., Huenges, E., 2018. The impact of reservoir heterogeneities on high-temperature aquifer thermal energy storage systems. A case study from Northern Oman. Geothermics 74, 150–162.
Witt, L., Moritz, J.M., Gröschke, M., Post, V.E.A., 2021. Experimental observations of aquifer storage and recovery in brackish aquifers using multiple partially penetrating wells. Hydrogeol. J. 29, 1733–1748.
Xiao, X., Jiang, Z., Owen, D., Schrank, C., 2016. Numerical simulation of a high-temperature aquifer thermal energy storage system coupled with heating and cooling of a thermal plant in a cold region. China. Energy 112, 443–456.
Zeghici, R.M., Oude Essink, G.H.P., Hartog, N., Sommer, W., 2015. Integrated assessment of variable density-viscosity flow for a high temperature mono-well aquifer thermal energy storage (HT-ATES) system in a deep geothermal reservoir. Geothermics 55, 58–68.
Zheng, C., Wang, P.P., 1999. MT3DMS: A modular Three-Dimensional Multispecies Transport Model For Simulation of advection, Dispersion and Chemical Reactions of Contaminant in Ground-Water systems; Documentation and User's guide. U.S Army Corps of Engineer Research and Development Center. Contract Report SERDP-99-1, University of Alabama, Vicksburg, Michigan, USA.
Zuurbier, K.G., Zaadnoordijk, W.J., Stuyfzand, P.J., 2014. How multiple partially penetrating wells improve the freshwater recovery of coastal aquifer storage and recovery (ASR) systems: a field and modeling study. J. Hydrol. 509, 403–441.